

Organic Electronic Devices Based on Polymeric Material and Tunable Photonic Crystal

— Organic LED, Conducting Polymer Laser, Organic Solar Cell, Organic TFT, Tunable Photonic Crystal, Tunable Laser, Photonic Liquid Crystal —

Katsumi Yoshino^{1,2,3,4}, Yutaka Ohmori³, Akihiko Fujii⁵, and Masanori Ozaki⁵

The historical background and recent progress in the development of organic electronics and photonic crystals, particularly tunable photonic crystals realized by combining photonic crystal structure with functional organic molecules, are discussed. The novel characteristics of organic electronic devices with mainly conducting polymers, which are related to the optical effects, and the tunable photonic crystals composed of periodic structures of optical wavelength order combined with functional organic materials are demonstrated.

KEYWORDS: organic material, conducting polymer, photonic crystal, liquid crystal

1. Introduction

Organic electronics, which utilize the novel electrical and optical properties of organic materials, such as π -conjugated molecules and polymers called conducting polymers, and photonic crystals (PCs) with periodic structures of optical-wavelength order, are considered to be key technologies for sustaining the highly advanced Information Society of the 21st century. The ubiquitous computing for sustaining such a society must be based on portable electronics and opto-electronics devices with light weight, flexibility, low energy consumption, low fabrication cost and high reliability.

In this paper, we discuss the historical background and recent progress in the development of organic electronics and PCs. In

particular, tunable PCs realized by combining the PC structure with functional organic molecules, as proposed by us, will be discussed in detail. In other words, in this article we discuss organic electronic devices based mostly on conducting polymers, restricting ourselves to fields related to the photonic effect and tunable PCs.

2. Organic Electronics

We can trace the origin of organic electronics back to the fundamental pioneering study of the electronic conducting characteristics of aromatic molecules such as anthracene and pentacene by Akamatu, Inokuchi, and Matsunaga.¹⁾ Since then, these aromatic molecules called organic semiconductors with conjugated π -electrons and their charge transfer complex have been studied in detail. On the other hand, in 1970, studies of conducting polymers with highly extended π -conjugated electron systems in the main chain of linear polymers became highly developed after the discovery of superconductivity in (SN)_x²⁾ and the insulator-metal transition in polyacetylene (CH)_x.³⁾ These π -conjugated polymers called conducting polymers, attracted great interest from both scientific and practical industrial viewpoints. Subsequently, various novel applications of conducting polymers have been proposed, which also stimulated fundamental studies of conducting polymers and the development of new conducting polymers. Conducting polymers can be considered to partially have the graphite structure which

is the first carbon materials used in electrical engineering by Edison, for example, as the filament of an incandescent lamp.

On the other hand, based on detailed studies of the unique dynamical, electrical, and optical properties of liquid crystals (LCs), LC display (LCD) devices have been extensively developed, and now cathode ray tube (CRT) display devices have been mostly replaced by LCDs. The low energy consumption and light weight of LCDs are essential for portable electronic devices. This success of LCDs utilizing organic LCs in electronics triggered the development of organic electronic and optoelectronics devices.

Simple and low-cost processes for the fabrication of organic devices are also attractive to engineers. For example, solution methods can be applied for large-area devices without the need for a vacuum system. It should also be noted that various types of organic materials with desired electronic band schemes can be molecularly designed and fabricated.

Organic devices can also be fabricated on various kinds of substrates, such as flexible polymers. That is, mechanical flexibility is another key advantages of organic devices.

There are so many fields in which organic devices may play important roles, but we will restrict ourselves to several examples such as organic light-emitting diodes (OLEDs), organic photodetectors (OPDs) and organic solar cells and organic thin film transistors.

Indeed, the applications of organic inte-

¹ Shimane Institute for Industrial Technology, Matsue 690-0816, Japan

² Collaboration Center, Shimane University, Matsue 690-0816, Japan

³ Innovation Center for Advanced Science, Osaka University, Suita, Osaka 565-0871, Japan

⁴ Department of Electrical and Electronic Engineering, Nagasaki Institute of Applied Science, Nagasaki 851-0193, Japan

⁵ Division of Electrical, Electronic and Information Engineering, Graduate School of Engineering, Osaka University, Suita, Osaka 565-0871, Japan

(Received March 7, 2007; accepted May 29, 2007; published online September 7, 2007)

©2007 The Japan Society of Applied Physics

graded devices, such as organic transistors, OLEDs and OPDs, in display panels and integrated plastic ICs, and organic sensor devices have been greatly progressing. The potential for commercialization is high for these organic devices because they are seen to compete in application areas where the market can incur costs in development. In portable and wearable electronic and optoelectronic devices and computers which are important devices in ubiquitous systems, organic devices would play the most important role.

OLEDs utilizing fluorescent dyes or conducting polymers are capable of emission over a wide visible range with high efficiency, and require only a low driving voltage. Recently, OLEDs that have a long lifetime and excellent durability have been realized for flat-panel display applications. There are some demands for the use of OLEDs not only in display applications but also as various light sources.

There are two types of devices, LEDs and lasers, for transmitting optical signals and/or energy. LEDs have lower power but are much less expensive than laser devices, and are used for short distances and multimode paths. The nanosecond transient electroluminescence of the blue OLED has also been reported. OLEDs can be expected to be applied to electro-optical conversion devices for generating high-speed optical pulses. OPDs utilizing copper phthalocyanine have been demonstrated to have a high-speed response. OPDs can also be applied to optoelectrical conversion devices for receiving high-speed optical pulses.

2.1 OLEDs

OLEDs have attracted great interest for thin film flat-panel display and solid state lighting device applications. An additional advantage of polymeric organic LEDs (PLEDs) utilizing conducting polymer is that they can be simply fabricated by wet processes, including ink-jet, and screen-printing methods, and other solution processes on various kinds of substrates including polymeric substrates for flexible devices.⁴⁾

Both PLEDs and emissive low-weight-molecule-based OLED have been developed by extensive utilization of initially, fluorescent materials and, later, phosphorescence materials.

For PLEDs, the introduction of side chains to linear conducting polymers was groundbreaking, because, with this introduc-

tion, conducting polymers became soluble and fusible, and their emission intensity was enhanced depending on the length of side chains.⁵⁻⁷⁾ In this respect, it should be mentioned that the synthesis of poly(9,9-dialkylfluorene) with a large band gap⁸⁾ and the first observation of blue electroluminescence (EL) in a PLED utilizing this material⁹⁾ stimulated the synthesis of this type of conducting polymer. That is, conducting polymers with desired band gaps could be designed and prepared to realize red, green and blue emission of PLEDs.¹⁰⁻¹²⁾ Particular effort has been expended for obtaining blue-emission PLEDs.

It should also be mentioned that the introduction of SP³ carbon or hetero-atoms such as Si and Sn in the main chain, as shown in Fig. 1, was found to be effective for increasing the

band gap in order to realize blue emission and for enhancing emission intensity by exciton confinement.^{13,14)}

The matching of the bottom of the conduction band and the top of the valence band of the conducting polymer to the Fermi energy levels of the cathode and the anode, respectively, in PLED devices is also important for achieving carrier injection. In particular, the introduction of nitrogen atoms to the structure was successful lowering the bottom of the conduction band to facilitate electron injection.^{15,16)}

To realize strong emission, it has been found to be effective to use phosphorescent materials.^{17,18)} That is, it is effective to enhance EL emission intensity by emissive recombination of triplet excitons. Here, we

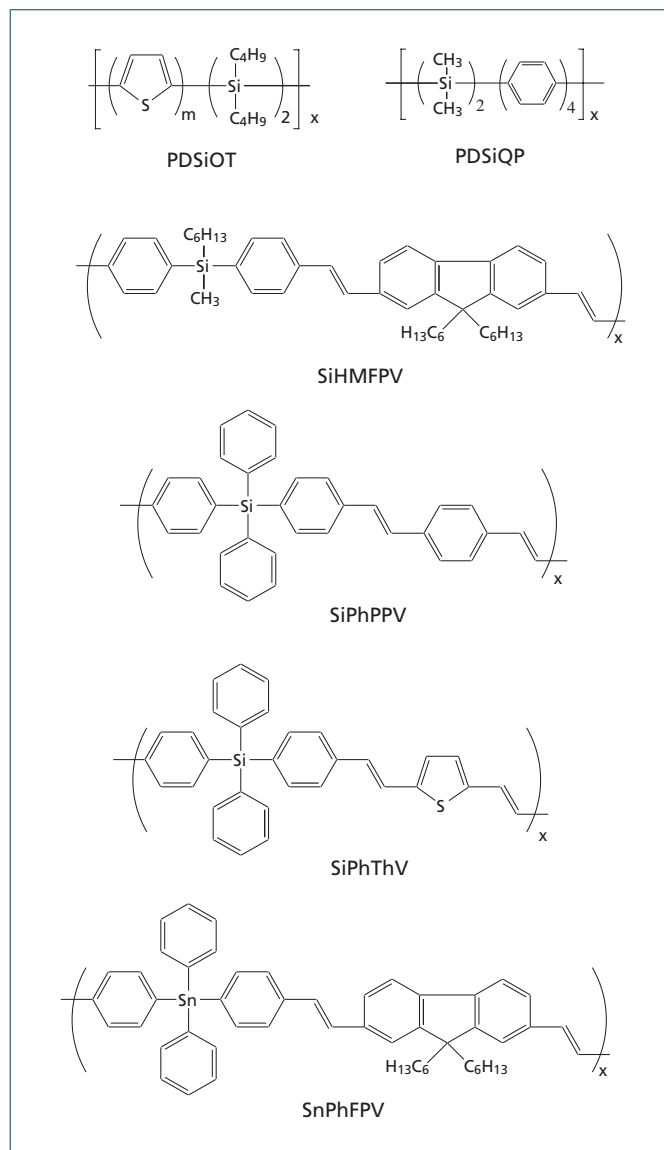


Fig.1 Molecular structures of conducting polymers with heteroatoms such as Si and Sn.

will only report recent results as examples. A low-molecular-weight phosphorescent OLED is usually fabricated by evaporation or molecular deposition in vacuum. However, for a practical low cost device, a wet process is desirable. Here, we will explain one of the trials as an example.^{19,20)}

Phosphorescent organic LEDs (PHOLEDs), fabricated using heavy-metal-containing phosphorescent compounds, exhibit high external quantum efficiencies and their radiative emission comes from the triplet states. In order to achieve high device performances, host materials with suitable triplet levels are needed to realize efficient energy transfer from the host to the dopants. For example, the green phosphorescent dye of bis(2-phenylpyridine)iridium(III) acetylacetonate [(ppy)₂Ir(acac)] doped into 3-phenyl-

4-(1'-naphthyl)-5-phenyl-1,2,4-triazole (TAZ) has been reported to show a peak internal quantum efficiency of nearly 100%.²¹⁾

Poly(*n*-vinylcarbazole) (PVCz) is used as a host material for PLEDs because of its high triplet level for some emitting phosphorescent complexes, and it shows high device performance. The starburst molecule, 1,3,5-tris[4-(diphenylamino)phenyl]benzene (TDAPB), has good hole transport characteristics owing to its highest occupied molecular orbital (HOMO) levels, and is expected to have triplet energy levels suitable as the host for the phosphorescent material Ir(ppy)₃. TDAPB is reported to be a starburst molecule with excellent hole-transporting characteristics for organic EL devices.²²⁾ In addition, TDAPB is resistant to crystallization because of its steric hindrance; it also possesses excellent wet-process film-forming

properties. Starburst molecules are useful; they combine the superior characteristics of small molecules and polymers such as sublimation of materials and wet-process film formation, and are expected to yield high-efficiency devices fabricated by solution processes.

The phosphorescent dye tris(1-phenylisoquinoline)iridium(III) [Ir(piq)₃] has been investigated for red PLEDs. We have used polymeric PVCz and starburst low-molecular-weight TDAPB as host materials in order to improve device performance by combining the advantages of a polymer and a low molecular weight. In addition, using the red phosphor results in exciplex emission between the host and carrier transport material (Fig. 2). We have employed two types of host materials for the efficient red PLEDs and have discussed the energy transfer from the host blend to the

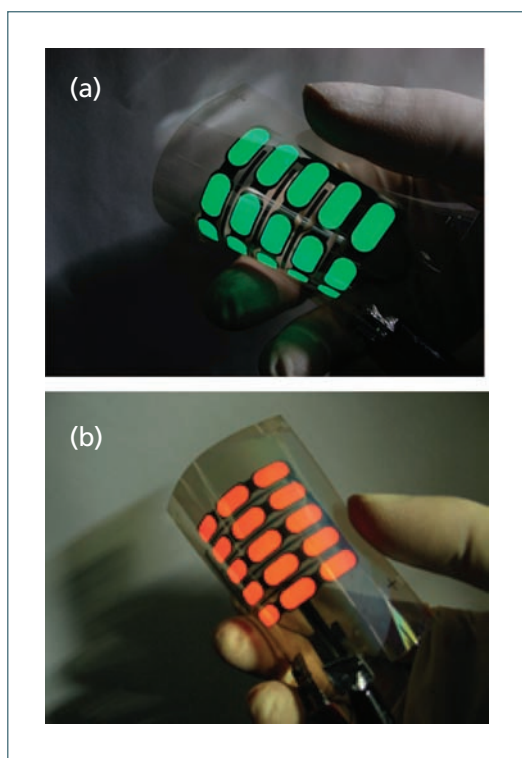


Fig.2 Photograph of flexible PLED with Ir(piq)₃.

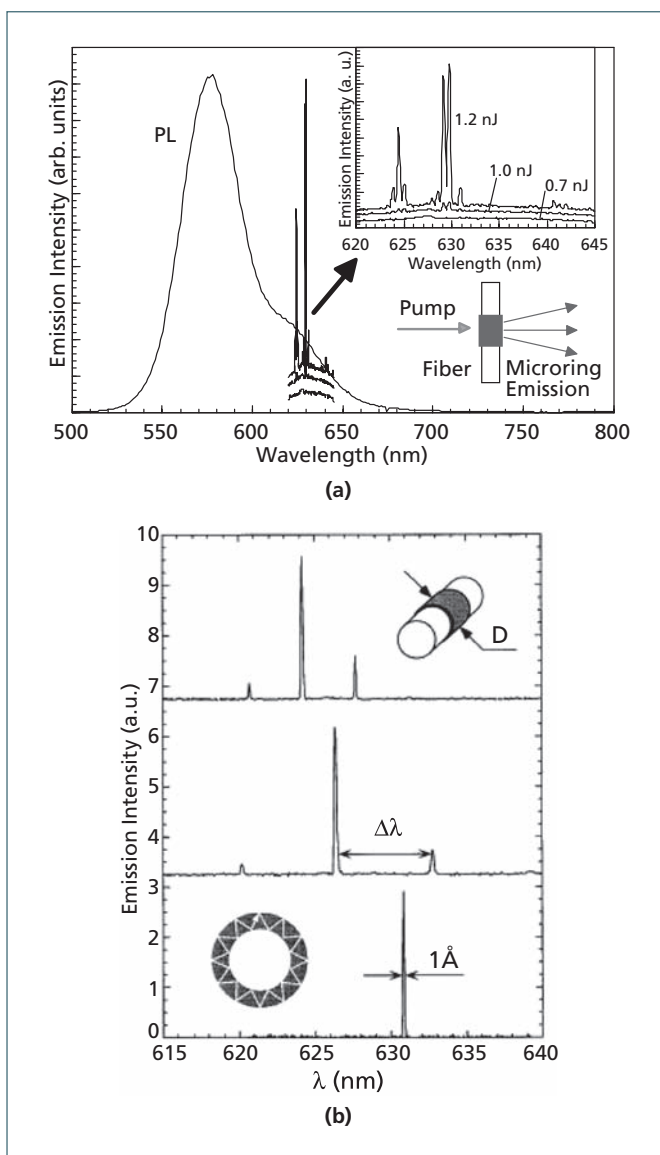


Fig.3 (a) Typical laser spectra and (b) single-mode emission of microring structure with conducting polymer.

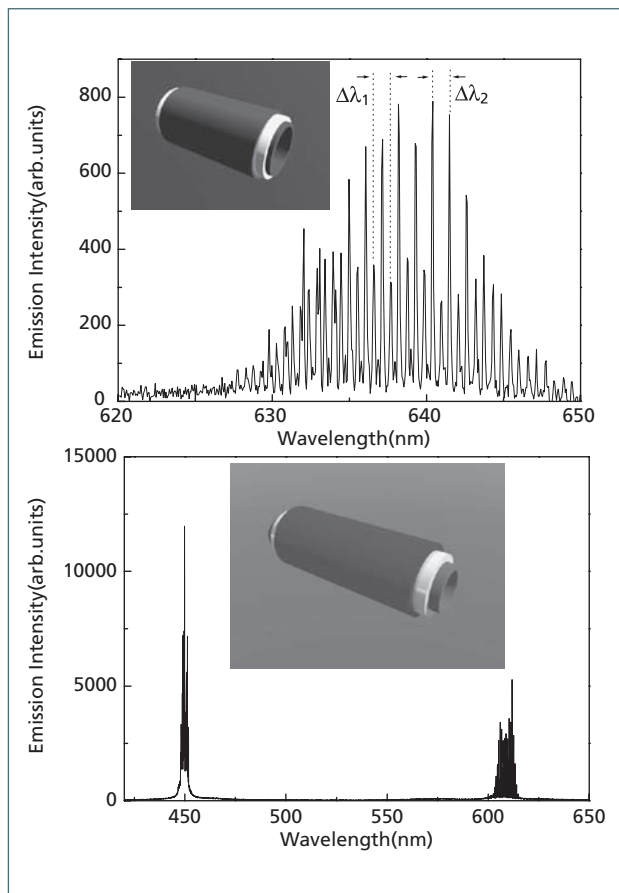


Fig.4 (a) Double-ring lasing and (b) dual-color lasing from microcapillary structure with conducting polymers.

dopant and the confinement triplet energy in the dopant.²³⁾

Usually, OLED is applied to flat panel displays. However, there are many other possibilities, for example, a light source in place of incandescent lamps or fluorescent lamps and also in optical communication. Here, we briefly mention that because of the wet-process fabrication technology of OLED, it can be fabricated directly on the end terminal of optical fibers. High-speed optical communication of video signals utilizing the OLED and the OPD with Cu-phthalocyanine have been successfully demonstrated.²⁴⁾

2.2 Conducting polymer laser

We have demonstrated that electronic energy schemes of conducting polymers best fit lasers because they are typical four-electronic-energy-level systems, with which we can realize population inversion and lasing with low threshold excitation.²⁵⁾

Indeed, even without outer cavity mirrors, super-radiation was observed upon optical excitation in conducting polymers.²⁶⁾ By the

introduction of fluorescent conducting polymers in cavities, low threshold lasing can be realized.²⁶⁾

We examined the microring structure of lasers by immersing optical fibers in solutions of conducting polymer. Then we were able to prepare microring structures surrounding optical fibers.²⁷⁾ A microring lasing device was also prepared by utilizing the microdisk structure on the substrate.^{28,29)} However, here, we restrict ourselves to microring fibers.

As shown in Fig. 3(a), the spectral width decreases drastically above a certain threshold excitation intensity. It should also be mentioned that upon decreasing the diameter of the fiber, single mode laser emission was observed, as

shown in Fig. 3(b).

We proposed the formation of microring structures utilizing glass pipes instead of fibers.³⁰⁾ In the case of pipes microrings can be formed not only on the outer surface of the pipe but also on its inside surface. The spectrum shown in Fig. 4(a) was obtained by

optical excitation on the double-ring device made of poly(2-methoxy-5-dodecyloxy-*p*-phenylenevinylene) (MDDOPPV).

By the analysis of Fig. 4(a), the emission was confirmed to originate from both outside and inside rings. It should also be stressed that by utilizing a different conducting polymer on the inside surface from that on the outer surface, two-color lasing can be realized, as shown in Fig. 4(b).³⁰⁾

2.3 Organic solar cells

There are two types of organic solar cells, donor-acceptor solar cells based on electron transfer between donors and acceptors, such as fullerene C₆₀ and their derivatives, and dye-sensitized TiO₂ cells, the so-called Graetzel solar cells.³¹⁾

The first type of solar cells resulted from our finding of photoinduced charge transfer between conducting polymers and C₆₀.³²⁻³⁴⁾ Here, we will discuss only this type of device.

As shown in Fig. 5, photoluminescence of conducting polymer is strongly quenched whereas photoconductivity is markedly enhanced upon the introduction of C₆₀ to the conducting polymer. These novel characteristics can be explained by photoinduced charge transfer between the conducting polymer and C₆₀.³²⁻³⁴⁾

Utilizing various combinations and structures of conducting polymers and fullerenes, various types of solar cells have been proposed, such as simple junction layers as well as others obtained by introducing new concepts such as photon-harvest molecules, and condensed interfaces, interpenetrating networks, and selective doping.³⁵⁻³⁷⁾

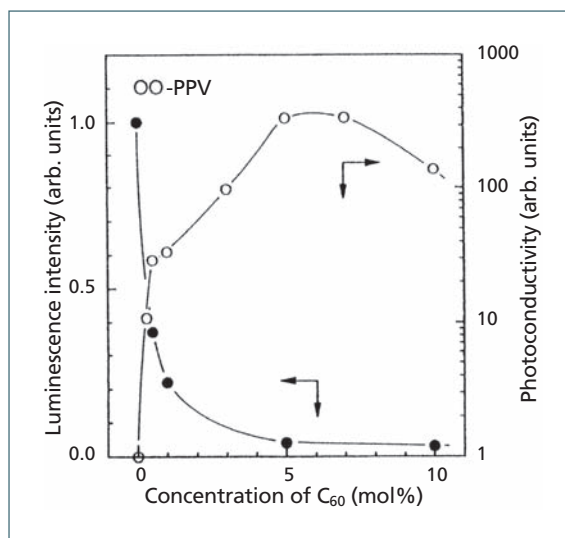


Fig.5 PL quenching and photoconductivity enhancement in composite system of conducting polymer and C₆₀.

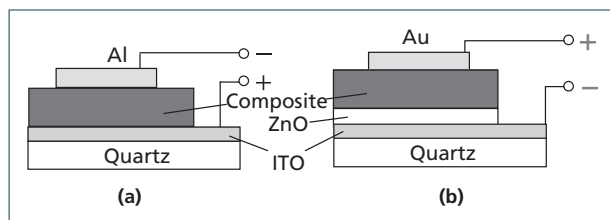


Fig.6 Schematic device structures of (a) conventional type and (b) inverted type with ZnO layer.

It should be mentioned that, compared with the conventional solar cells shown in Fig. 6(a), in which light impinges from the indium tin oxide (ITO) electrode side on which the conducting polymer layer is formed, in the inverted structure of the device shown in Fig. 6(b), the conversion efficiency was increased markedly owing to the suppression of the window effect of the conducting polymer.³⁸⁾ That is, by utilizing a transparent ZnO electrode on which a C₆₀ layer is formed and irradiating from this side, the window effect was eliminated, because electron-hole separation occurs at the interface between C₆₀ and the conducting polymer junction.³⁹⁾

It should also be mentioned that in the interpenetrating network type of solar cells of simple structure, by optimizing the dispersion of C₆₀ in conducting polymer by various methods such as annealing, high efficiency was also attained, as shown in Fig. 7.⁴⁰⁾

2.4 Organic thin film field-effect transistors and others

Organic field-effect transistors (OFETs) fabricated with the conducting polymer, polythiophene, on Si substrates were reported by Koezuka *et al.*⁴¹⁾ On the other hand, we reported FETs on polymer substrates.⁴²⁾ It should also be mentioned that in our junction devices utilizing poly(3-alkylthiophene), which exhibits thermochromic behavior, strongly temperature-dependent characteristics were observed.⁴³⁾ After those reports, many papers on the FET were published. To apply wet processes, soluble conducting polymers have been preferred. On the other hand, to obtain high carrier mobility, low-molecular-weight aromatic molecules have been preferred and used. Therefore, a method of applying wet processes to aromatic molecules as well as oligomers has been sought.

The high performance of OFETs fabricated from an annealed pentacene solution and organic transistors with solution-processed

source/drain electrodes using metal nanoparticles have been reported.

The thiophene oligomers with high carrier mobility are candidates for realizing all-organic circuits on an active semiconductor layer. A high mobility of greater than 0.1 cm²/(V·s) can be obtained from oligothiophene transistors fabricated by dry processing. OLEDs with oligothiophene as the hole-transporting layer have been reported.

On the other hand, soluble poly(3-alkylthiophene) is one of passes from the liquid phase to the solid phase. OFETs fabricated by casting show higher field, making them promising materials for large-area devices. The field-effect mobility of polymer transistors fabricated by wet processing is more strongly dependent on the self-organized structure, which is influenced by the polymer solution, than that of transistors fabricated by spin coating. Various bipolar-type OFETs based on composites of p-type conducting polymers and n-type dyes have been fabricated by spin-coating. It is also of interest to examine the OFETs having composites of conducting polymers and dyes with the same backbone.⁴⁴⁾

Organic chromic devices are also promising for applications in various fields.

We have proposed a color switching device based on the reversible insulator-metal transition occurring in conducting polymer upon doping and undoping.⁴⁵⁻⁴⁷⁾ This idea came to us when a drastic change in electrical conductivity owing to insulator transition upon doping was discovered,⁴⁵⁻⁴⁷⁾ because we had expected a color change from that conducting polymer in the insulating state to a metallic color in the metallic state resulting from plasma reflection. Indeed, dramatic change in color and excellent characteristics of color switching in conducting polymer as were expected. The color depends on the kind of conduction polymer. For example, polythiophene switches between red in the insulator phase to blue in the metallic state. Multicolor changes can be realized in polyaniline and other conducting polymers. The switching speed is faster than those of conventional nematic LC (NLC) devices. The life exceeding 10⁵ cycles can be demonstrated.⁴⁵⁻⁴⁷⁾ To be widely used, a longer cycle life is necessary, and the use of an ionic liquid has been reported to be one of the methods of improvement.⁴⁸⁾

By designing an appropriate molecular structure of the conducting polymer and

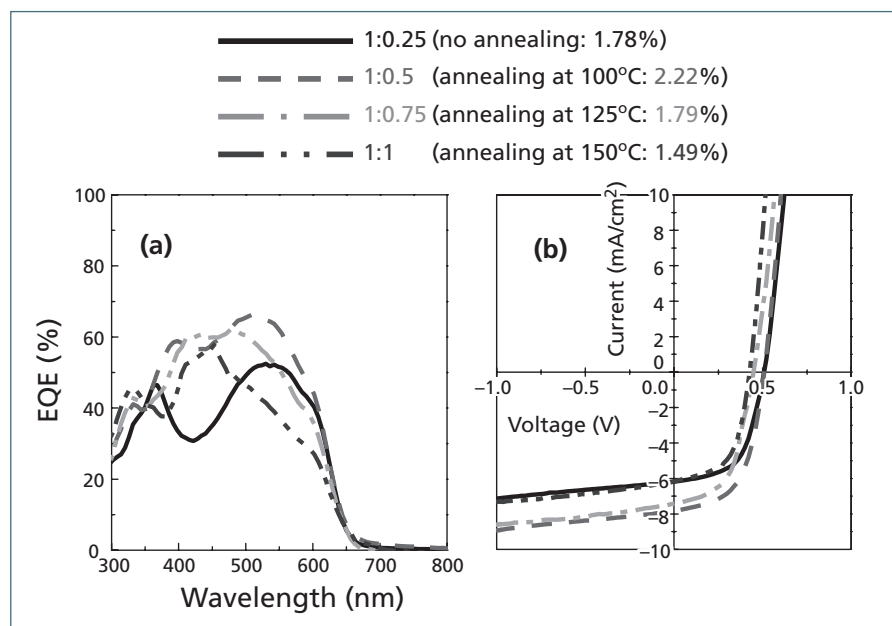


Fig.7 EQE spectra and *I-V* characteristics of thin-film solar cells with composite system of conducting polymer and C₆₀ obtained under various postdeposition annealing conditions.

device structure and system, a full-color, reliable long-life optical device should be realized in the near future.

3. Photonic Crystal

Recently, PCs with a three-dimensionally periodic structure of the order of optical wavelengths have attracted great interest, because in this new class of material novel concepts such as a photonic band gap (PBG) in the energy range of which photons cannot exist or propagate. Upon the introduction of defects, localized states at which photons can localize are formed in the PBG. That is, PBG materials are a new class of ordered structures with a periodicity of optical-wavelength order, which facilitates the manipulation of photons in the same way that a semiconductor controls the flow of electrons.^{49,50} The propagation of photons in such PCs is similar to the propagation of electrons in semiconductors. The PBG in a PC plays, for photons, the same role as the forbidden energy gap for electrons in semiconductors, thereby allowing the manipulation of light flow. Hence, optical devices that are analogous to semiconductor devices are made feasible by this phenomenon. As a consequence, PBG devices have the potential for accomplishing for optical circuitry what semiconductor devices have done for electrical circuitry. A number of unusual optical properties are predicted in PCs. In particular, the study of stimulated emission in the PBG is one of the most attractive subjects, since, in the PBG, spontaneous emission is inhibited and low-threshold lasers based on PCs are expected.^{49,51-54} In order to realize PCs, a large number of intensive studies on microfabrication based on semiconductor processing technology⁵⁵⁻⁵⁷ and self-assembly construction of nanoscale spheres^{58,59} have been carried out.

Silica opal is a type of naturally occurring PC that consists of well-ordered three-dimensional (3-D) arrays of SiO₂ spheres, that have diameters in the range of visible wavelengths. Indeed, the iridescent coloration of such opals is caused by the diffraction of light from these regular arrays of silica particles of monodispersed diameter of optical-wavelength order.

3.1 Fabrication of 3-D PC: synthetic opal and inverse opal

Synthetic opals are prepared by the following process. Monodispersed silica colloidal spheres are synthesized in aqueous

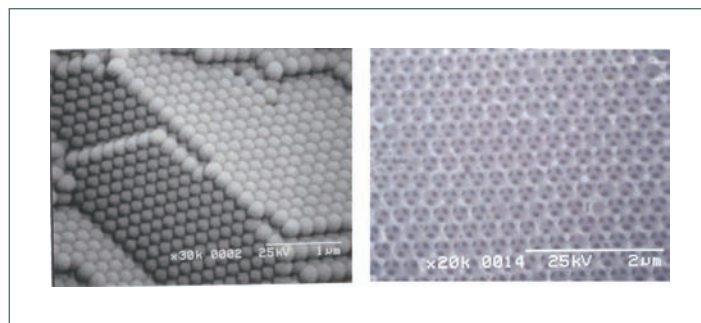


Fig.8 SEM image of plastic opal and inverse opal.

solutions by well-known procedures. Ordered colloidal crystals having various PBGs can be prepared by sedimentation of the suspension of monodispersed SiO₂ spheres of various diameters. These crystals are annealed at 100–120°C and sintered at 600–700°C to induce a small degree of interparticle sintering, which mechanically stabilizes the structure. These mechanically robust, porous opals are cut into plates. Thin film of synthetic opal can also be formed by sedimentation of SiO₂ spheres in a sandwich cell made of two glass plates with a separation of several to hundreds μm. Porous opal prepared by this procedure has a fcc crystal lattice structure, which is sometimes faulted with hexagonal-close-packed stacking arrangements. Polymer opals are also prepared directly utilizing polymer spheres of nanosize in diameter (Fig. 8). As evident in the scanning electron microscope (SEM) image, in this opal, regular stacks of silica spheres were confirmed. Figure 9 shows the transmission and reflection spectra of the synthetic opals prepared by this method. As

clearly shown in this figure, clear reflection peaks and transmission dips were observed depending on the size of the spheres, which indicates the regular periodic array of particles. The peak and the dip correspond to the band gap of the 3-D PC of opal.

The opal prepared by this procedure contains an interconnecting structure of tetrahedral and octahedral voids. These voids are fully interconnected by channels through hexagonal close-packed layers. Inverse opals can be prepared by filling the voids with secondary materials such as liquid photopolymer and consequently removing silica particles by HF etching. Carbon inverse opals with 3-D periodicity can be prepared by infiltrating phenol resin and subsequently removing silica using HF, followed by annealing for carbonization. Carbon can also be directly infiltrated in voids by chemical vapor eposition (CVD). For example, propylene (C₃H₆) is chosen as the precursor gas in order to increase the reaction yield in the CVD process.⁶⁰

As clearly shown in Fig. 8(b), regular

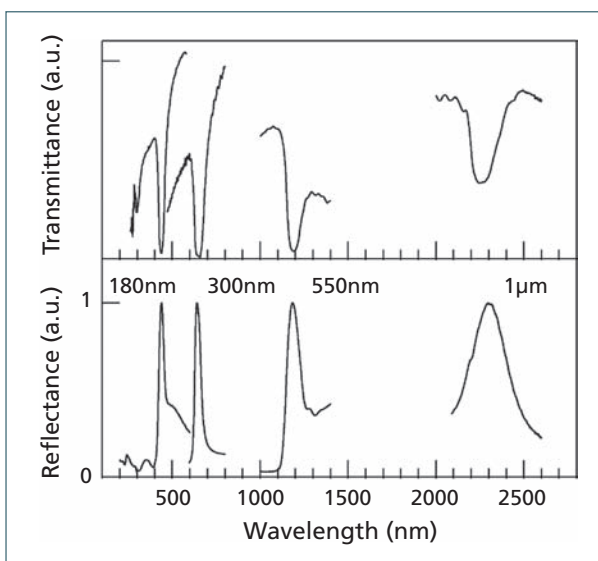


Fig.9 Transmission and reflection spectra of synthetic opal formed from silica particles with various diameters.

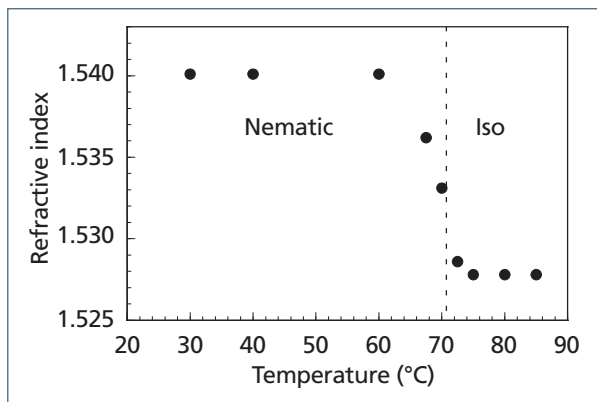


Fig.10 Refractive index of nematic liquid crystal evaluated by stop band analysis.

arrays of voids were observed in inverse opal. The size of voids depend on the diameter of silica spheres.

3.2 Tunability of optical properties in opal-based PCs

We have combined experimental and theoretical studies to devise and evaluate new types of PCs: tunable PCs (TPCs) based on synthetic opals. The TPCs consist of periodic particle arrays which provide either optical or electrical tunability for the properties of the PC, particularly the width and position of the PBG. The tunability can be realized by changing the periodicity, crystal structure, or refractive index, for example. One of the methods of changing the refractive index of PCs, synthetic opals with SiO₂ spheres, is to infiltrate various active materials, such as metals, semiconductors, organic molecules and polymers, into the nano-scale voids of the opals.⁵⁸⁾ TPCs are expected to combine the advantageous properties of conventional PCs with the tunability of the refractive indices of such active materials as conducting polymers, photoresponsive materials, and mesogenic materials. Modifications of the periodicity and crystal structure can also be realized by applying mechanical stress to plastic opals fabricated by the sedimentation of nanoscale polymer spheres. Various new functionalities are expected in these TPCs made of infiltrated opals and inverse opals.

3.2.1 Temperature tuning

Temperature tuning of the optical properties of PCs has been achieved by various approaches. We have demonstrated the temperature tuning of the stop band of the reflection spectrum a) by heat treatment at

temperatures higher than 900°C, b) upon refractive index change at the phase transition temperature in LC-infiltrated opal, and c) due to the thermochromism of conducting polymers infiltrated in a synthetic opal.

a) Heat treatment of SiO₂ opal

The stop band position of SiO₂ opal can be tuned via the effect of heat treatment. Upon heat treatment at temperatures higher

than 900°C, reflection spectra change with changing treatment period T_h . Bragg diffraction peaks at each incident angle shift to shorter wavelengths with increasing T_h , which can be interpreted in terms of the decrease of periodicity. That is, the lattice constant evaluated from the analysis of diffraction peak decreases monotonically with increasing heat treatment period T_h , which were consistent with the electron microscope observation and can be interpreted to be due to the progress of sintering. From these results, it has been confirmed that the effective lattice periodicity of PCs can be tuned at any value in a wide range by heat treatment.⁶¹⁾ It should also be noted that the pore size of opals can also be controlled by heat treatment, which should also influence the infiltration of foreign material and its characteristics.⁶²⁾ It should be noted that this type of tuning is permanent.

b) LC-infiltrated opal

The stop band of opals infiltrated with LCs, such as NLC and smectic LC, shows a marked shift with changing temperature. It should also be mentioned that the wavelength of the stop band shifts stepwise at the phase transition points between various phases, which can be interpreted in terms of the change in refractive index. As shown in Fig. 3, the refractive index of NLC (ZLI-1132) evaluated by the analysis of the stop band shows

stepwise changes at the phase transition points, which is consistent with the directly measured refractive index of various phases. It should also be mentioned similar stepwise change of the stop band was also observed in PCs of smectic-LC-infiltrated opals, as shown in Fig. 10. That is, these results indicate the possibility of the temperature tuning of PCs of LC-infiltrated opals.

Phase transition behavior of LC was also confirmed to change when it was infiltrated to nanovoids in the opal from dielectric measurements. The dispersion frequency of the dielectric constant of NLC in the nanosize voids in the opal is higher in frequency by about one order of magnitude than that in a conventional sandwich cell, which is consistent with the faster response speed of the electrooptic effect in the opal infiltrated with LC. This may originate from the strong interaction of LC molecules with the inner surface of the nanoscale voids in the opal, resulting in the strong recover force. It should be mentioned that this tenability in LC-infiltrated opal is reversible.

c) Thermochromism of conducting polymers infiltrated into opal

We proposed the novel temperature tuning method of the optical stop band using the change in the refractive index associated with the thermochromism of conducting polymer infiltrated into synthetic opals. Figure 11 shows the transmission spectra of a synthetic opal infiltrated with poly(3-octadecylthiophene) (PAT-18) as a function of temperature. As is evident from this figure, the wave-

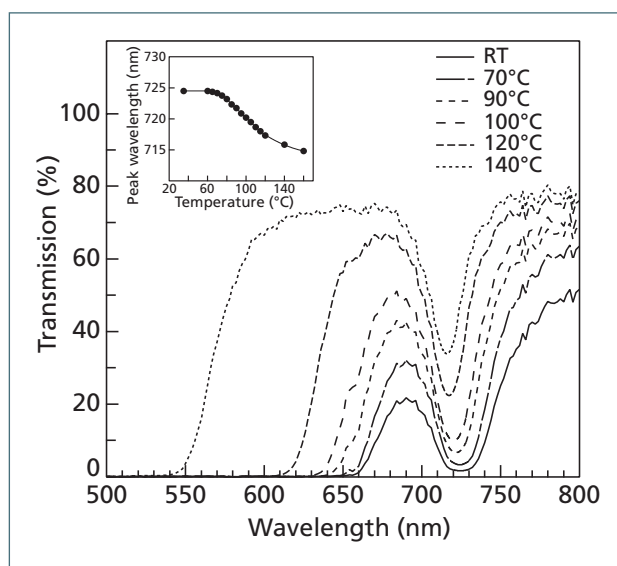


Fig.11 Transmission spectra of opal thin film infiltrated with PAT-18 as a function of temperature. The inset shows temperature dependence of peak wavelength of transmission spectra.

Fig.13 (a) Reflection spectra of LC-infiltrated polymer inverse opal as a function of applied voltage. (b) Peak reflection wavelength and effective refractive index of LC in voids as a function of voltage.

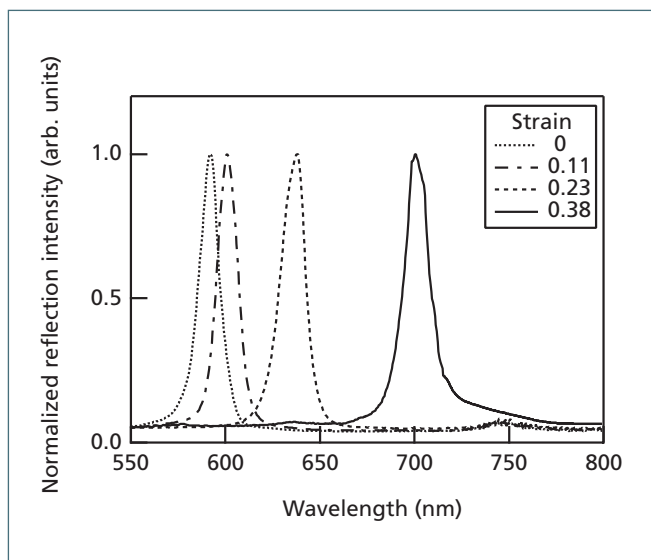
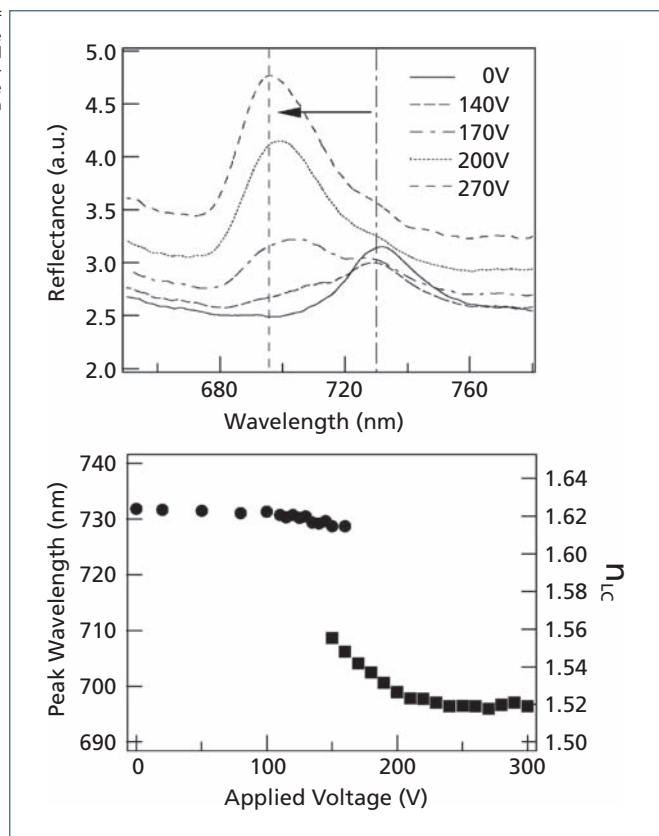


Fig.12 Reflection spectra as a function of applied mechanical stress.



length of the stop band shifts considerably with increasing temperature. For example, at the wavelength of 725 nm, the transmittance can be varied from 1.6% (room temperature, RT) to 47% (140°C) by changing the temperature. It should be noted that these shifts of the transmission spectra with temperature were confirmed to be reversible. The change in the refractive index of PAT-18 evaluated from the change in the stop band with increasing temperature coincides with that of the directly estimated value. That is, the blue shift of the peak wavelength of the stop band can be attributed to the decrease in the refractive index of PAT-18 which is due to the increase of the band gap of PAT-18, with increasing temperature.

3.2.2 Mechanical tuning in plastic opal

The periodicity and filling factor of the opals and infiltrated opals can be controlled by applying mechanical stress. In the case of silica opal, upon applying pressure, we can observe a change in the periodicity, which results in the change of the optical properties such as the stop band position in the transmission spectrum.

In the case of polymer opals, particularly

opals made of elastomer spheres, we can reversibly change the optical properties by applying mechanical stress. As shown in Fig. 12, the reflection peak of the plastic opal is confirmed to shift drastically upon the application of uniaxial mechanical stress perpendicular to the light beam. This effect can be explained as a change in the periodicity in the direction of the light beam. That is, the reflection peak exhibited large redshift upon the application of pressure, owing to the increase in the periodicity in the direction of light beam. On the other hand, the reflection peak exhibited blue shift as a result of stretching due to the decrease of the periodicity in the direction of the light beam. These results suggest the possibility of mechanical tuning of the PC. Mechanical tenability was also demonstrated in elastomeric-polymer inverse opal prepared by the replica method.

3.2.3 Voltage tuning

Voltage tuning can be realized in synthetic PAT-infiltrated opal used as one of the electrodes in an electrochemical cell. Upon electrochemical doping of the conducting polymer infiltrated into the opal, the shift of the reflection peak was observed. By analyzing the

reflection peak as function of the electric field, the observed results can be explained in terms of the change in the refractive index of the conducting polymer infiltrated into opals upon electrochemical doping of BF_4^- ions. This result indicates the possibility of voltage tuning of PCs.

On the other hand, LCs have a high optical anisotropy and are sensitive to external stress such as an electric field. Because of such optical anisotropy and field sensitivity, TPC has been proposed to be made of opal or inverse opal infiltrated with LC. In the LC-infiltrated opal thin film made of SiO_2 spheres, the stop band shift upon voltage application was confirmed. This is interpreted to originate from the refractive index change due to the molecular reorientation caused by the voltage application.

Figure 13(a) shows reflection spectra of the polymer inverse opal infiltrated with 5CB as a function of the amplitude of applied rectangular voltage ($f=1$ kHz). The light was irradiated perpendicularly to the replica film, i.e., in the [111] direction. As is evident from this figure, the reflection peak shifts to shorter wavelengths with increasing voltage. This has been interpreted to be due to the refrac-

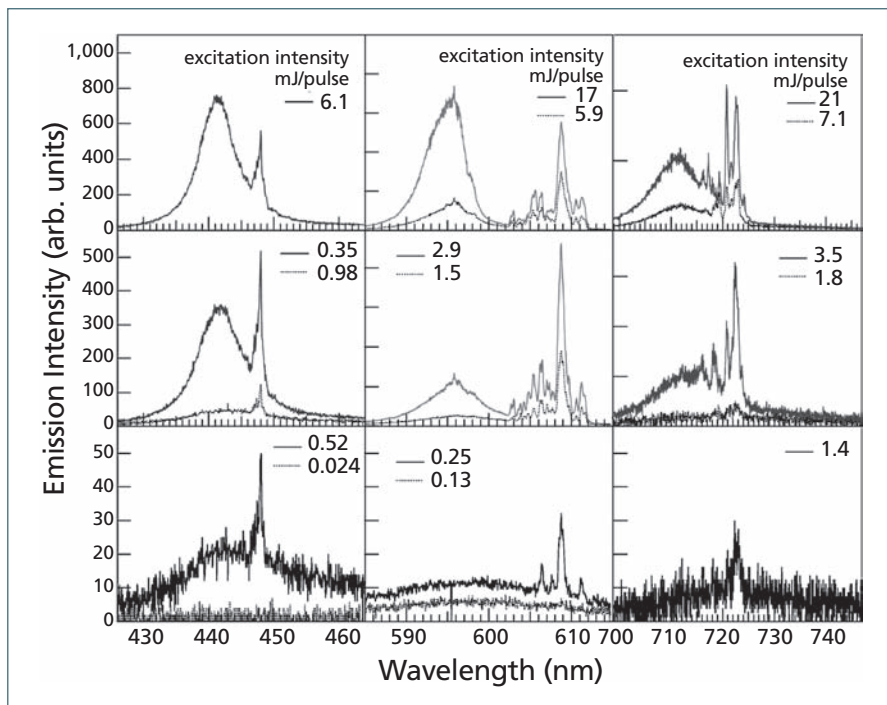


Fig.14 Emission spectra of MDDO-PPV as a function of excitation intensity in green opal infiltrated with THF.

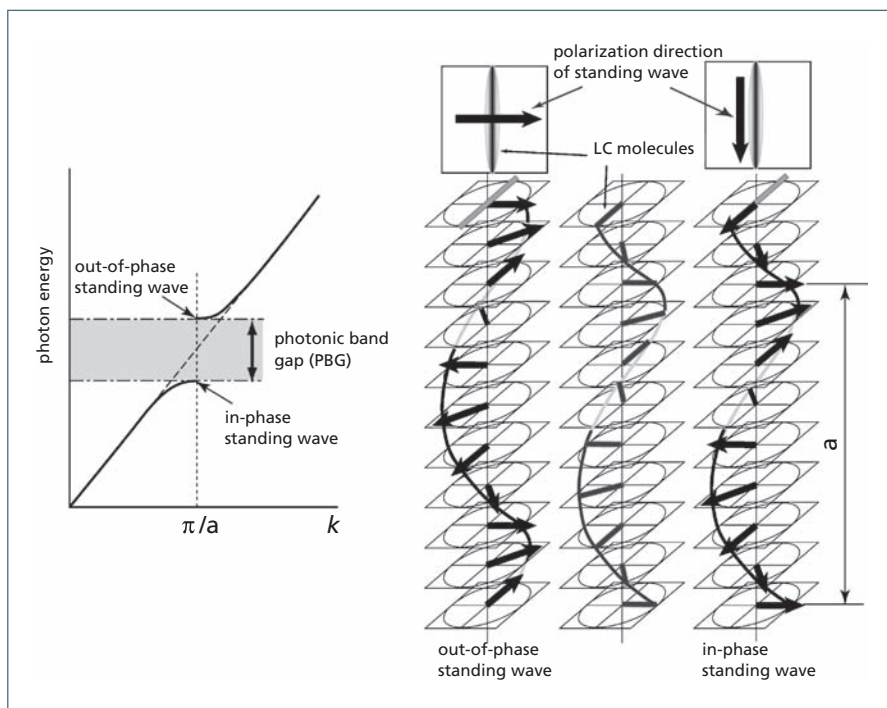


Fig.15 Schematic explanation of the appearance of photonic band gap in spiral periodic structure.

tive index change caused by the molecular reorientation along the applied electric field. In the initial state, the refractive index of LC filled into nanosize voids in the opal should be macroscopically averaged and is equivalent to that in the isotropic phase, because of the 3-D symmetry of the arrangement and shape of the voids without electric field. Under applied electric field, however, the LC molecules align along the field parallel to the direction of light propagation, and the ratio of the molecules aligning parallel to the direction of light propagation slightly increases. As a result, the component of the refractive index n_o for ordinary light increases in each void, and the averaged refractive index of LC decreases. Consequently, the reflection peak shifts to shorter wavelengths. A similar behavior, that is, the shift of the peak position of the reflection spectrum upon applying voltage, has also been observed in silica opal infiltrated with LC.

Figure 13(b) shows the voltage dependence of the reflection peak wavelength λ_{LC} of the polymer inverse opal infiltrated with 5CB. The total shift of λ_{LC} upon the application of 300V is about 35nm, which is much larger than that of the silica opal infiltrated with 5CB. This should be attributed to the large volume fraction of the voids filled with LC, the refractive index of which changes upon the application of voltage compared with that in the silica opal.

The orientation of directors of LCs changes upon applying magnetic field. Therefore, magnetic field tuning of reflection and transmission in opals infiltrated with LCs can be realized.

In the above-described electric field and magnetic field tuning of PC characteristics in LC-infiltrated opals, any LCs, such as NLC, smectic LC, and cholesteric LC, can be used. On the contrary, opals infiltrated with LCs can be used as optically detectable magnetic field sensors.

3.2.4 Optical tuning

The optical properties of materials that have been infiltrated into synthetic opals and that also constitute opal replicas can also be controlled by light irradiation. We have demonstrated that the optical property of PCs infiltrated with photochromic molecules or polymers and polymers containing photochromic moieties such as azobenzene in the side chains can be controlled by light irradiation. In this case, we can either permanently or

transiently control the PC by light irradiation. Materials that exhibit photoinduced phase transition are also interesting for infiltration into synthetic opals.

3.2.5 Solvent effects

To clarify the possibility of tuning the stop band of opals used as PCs, the shift of the stop band and the diffraction peak were studied as a function of the refractive index of the solvent. The reflection peak shifts drastically upon changing the solvent. The wavelength of the reflection peak increases with increasing refractive index of the solvent. These findings suggest the possibility of tuning the PBG in the infiltrated PCs.

3.3 Enhancement of spectral narrowing and lasing by infiltration into opal

We have reported the observation of the inhibited spontaneous emission of an organic dye, rhodamine 6G, infiltrated in a polymer replica of synthetic opal as a PC. The morphology-dependent resonances, superimposed on the broadband emission of rhodamine 6G owing to spherical wavelength-sized microcavity enhancement of dye emission, have been observed.

The spectral narrowing of photoluminescence (PL) and the evolution of sharp emission lines upon optical excitation have also been observed in opals made of SiO₂ spheres infiltrated with conducting polymers such as poly(2-methoxy-5-dodecyloxy-*p*-phenylenevinylene) (MDDOPPV) and also fluorescent dyes such as rhodamine 6G, NK-3483, and coumarin 120. The lasing characteristics were found to be dependent on the combination of the dyes and conducting polymers as well as the periodicity of the opal and also the refractive index of the solvent. Lasing was observed when fluorescent dyes exhibiting green PL, red PL, and purple PL were infiltrated in green opal, red opal, and purple opal, respectively. These results suggest that the periodicity of the opal plays an important role in lasing.

Figure 14 shows the emission spectra of the purple, green and red opals infiltrated with THF solution of coumarin 120, MDDO-PPV, and NK-3483, respectively, as a function of excitation intensity. With increasing excitation intensity, the PL peak became markedly enhanced in intensity and the spectral width became much narrower. In addition, sharp new emission lines appear. The former can be

explained by the amplified spontaneous emission (ASE) and the latter by multimode lasing (ML) influenced by the optical feedback due to the periodic structure of the opal matrix.

4. Photonic Crystal based on Self-Organized Helix Structure of Chiral Liquid Crystals

LCs including a chiral molecule have a self-organized helical structure that can be regarded as a one-dimensional (1-D) periodic structure and shows characteristic optical properties.⁶³ In such systems with a helix, light propagating along the helical axis is selectively reflected, depending on the polarization states, if the wavelength of the light matches the optical pitch of the helical structure, this is called selective reflection. The wavelength region in which the light cannot propagate is the stop band, and is considered the 1-D pseudo-band gap. Lasing at the band edge has been reported in the cholesteric LC (CLC),^{64,65} chiral smectic LC,⁶⁶⁻⁶⁸ and polymerized cholesteric LC (PCLC).^{69,70} These laser actions in the 1-D helical structure of chiral LCs are interpreted to be based on the band edge of the 1-D photonic band gap in which the photon group velocity is suppressed.⁷¹

4.1 Photonic band gap and band edge lasing in CLC

In the helical periodic structure of the CLCs, light propagating along the helical axis is selectively reflected, depending on the polarization states. If the wavelength of the light matches to the optical periodicity of the helical structure, this is called selective reflection. In this case, there are two types of circularly polarized standing waves with zero group velocity at the edges of the stop band, as shown in Fig. 15. Here, the rods indicate the molecular long axes of the CLC molecules and the arrows show the polarization direction of the standing waves. For one standing wave, the polarization direction of the light is parallel to the molecular long axis and, if we dope a laser dye, the polarization becomes parallel to the transition moment of the doped dye. This light is subjected to the extraordinary refractive index of the LC and has lower energy with respect

to a traveling wave, which corresponds to the longer edge of the stop band. Moreover, this circularly polarized standing wave effectively interacts with the laser medium and we can expect the low threshold laser action at the longer wavelength edge of the band gap.

4.1.1 Electrical tunability of lasing wavelength in dye-doped ferroelectric LC

Chiral smectic LCs with a tilted structure show a ferroelectricity, and are called ferroelectric LCs (FLCs). They are promising for electrooptic applications because of a fast response to the electric field.⁷² The FLC also has a helical structure and shows selective reflection due to the 1-D periodic structure in almost the same manner as the CLC.⁷³

Figure 16 shows emission spectra of dye-doped FLC as a function of pump energy. For low pump energy (1.76 μJ/pulse), the spectrum is dominated by a broad spontaneous emission and a dip is observed in the broad spectrum. The dip originates from the selective reflection band resulting from the helix of FLC. As the excitation energy increases, the emission intensity is enhanced. At a high excitation energy (10.4 μJ/pulse), lasing becomes evident as a sharp peak at the lower energy edge of the dip. The full width at half maximum (FWHM) of the emission peak is less than 0.5 nm. The laser light emitted from the FLC is circularly polarized and the sense of the polarization is right-handed, which coincides with the helical sense of the FLC used here. This strongly supports the idea that the laser action in the dye-doped FLC is based on the band-edge effect in the periodic structure of the FLC helix.

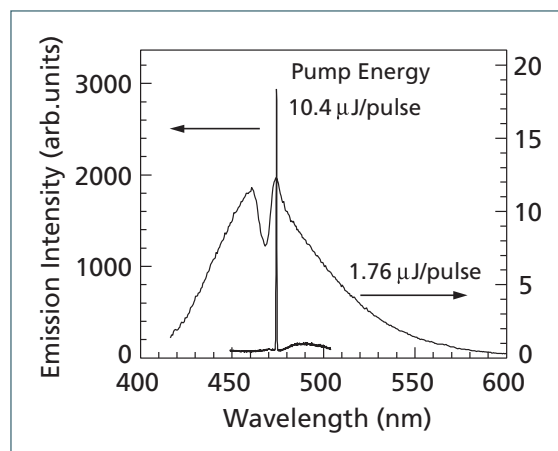


Fig. 16 Emission spectra of dye-doped FLC as a function of pump pulse energy.

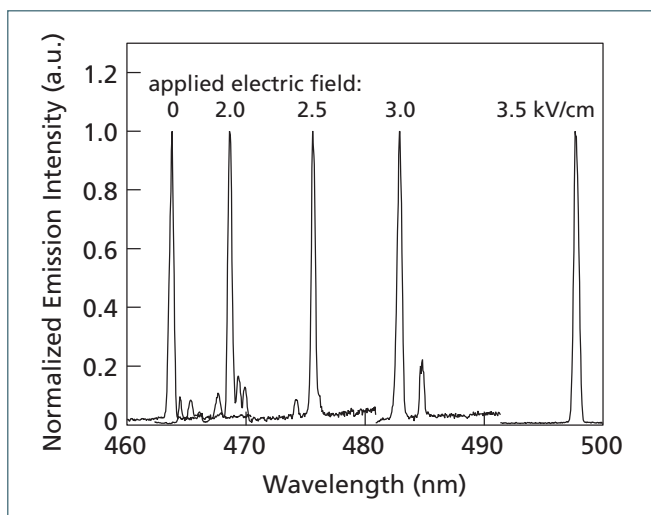


Fig.17 Normalized emission spectra at high excitation energy in dye-doped FLC as a function of applied electric field.

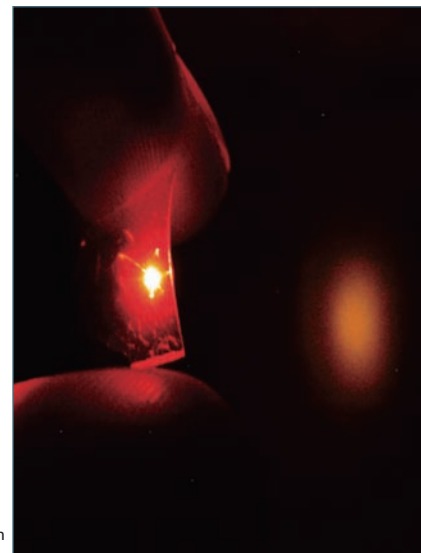


Fig.18 Laser emission from bent film of polymerized CLC.

The helix of FLC can be easily deformed by applying electric field and its response is fast because of the strong interaction between the spontaneous polarization and electric field. FLC has a spontaneous polarization P_s normal to the molecules and parallel to the smectic layers. When the electric field is applied in the layer, for lower field, P_s tends to point along the field direction and FLC molecules start to reorient toward the direction normal to the, resulting in the deformation of the helix. In the equilibrium state, the deformation of the helix might cause the elongation of its periodicity. Above the threshold field, all FLC molecules orient towards the same direction and the helix is unwound. The fact that the periodicity of the helical structure of the dye-doped FLC can be controlled by applying an electric field prompts us to expect the possibility of electric field tuning of the laser emission wavelength. Figure 17 shows the lasing spectra of the dye-doped FLC at high excitation energy

(24 $\mu\text{J}/\text{pulse}$) as a function of the applied electric field. It should be noted that lasing wavelength shifts greatly towards longer wavelengths with increasing field, which corresponds to the shift of the selective reflection band. In spite of a weak field (3.5 kV/cm), wide tuning of the lasing wavelength was achieved.

Lasing in the FLC mentioned above has been performed in the cell configuration in which the helical axis is perpendicular to the substrates and laser light is emitted perpendicularly to the cell surface. In this configuration, the pump beam is absorbed in the vicinity of the interface between the LC and the substrate, and doped dye in the bulk is not effectively excited. We have designed a planar cell configuration of dye-doped FLC for lasing, in which the helix axis is parallel to the substrates, and demonstrated optically pumped lasing in a waveguide.⁶⁸ Also in this waveguide LC laser, the emission wave-

length can be controlled over a wide range by applying electric field.

4.1.2 Laser action in photopolymerized CLC

Optically pumped laser action has been observed in a dye-doped flexible freestanding film of photopolymerized CLC (PCLC). In the PCLC film, the self-organized helical structure acts as a 1-D PC. At a high excitation intensity above the threshold, laser action is observed at the edge of the 1-D photonic band of the PCLC helical structure. This PCLC film laser possesses an excellent mechanical flexibility, and the laser action is also observed in a bent film of PCLC, as shown in Fig. 18. This implies that the 1-D periodic structure needed for the laser action is maintained even in the deformed film. Using such flexibility of the PCLC film, a focusing effect of laser emission is demonstrated in a circularly deformed film. Moreover, the helical pitch of the PCLC has no temperature dependence, in contrast to that

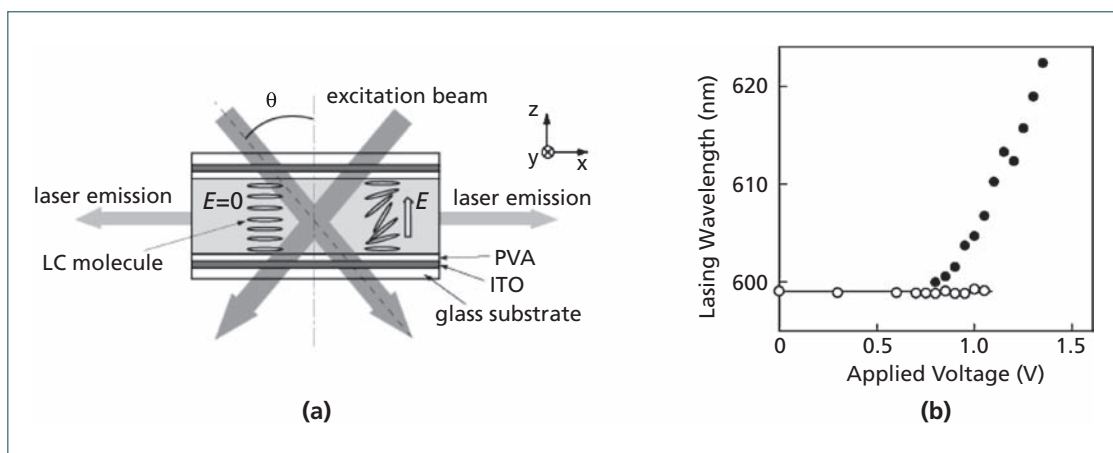
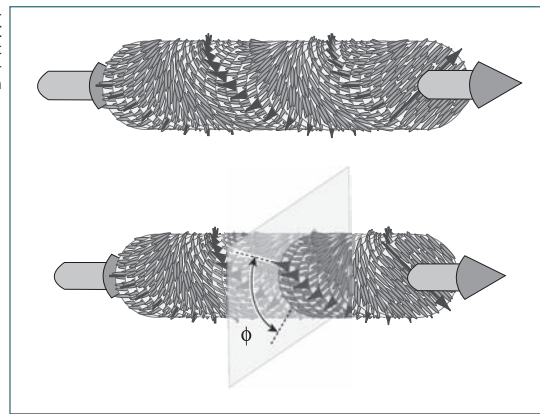


Fig.19 (a) Schematic explanation of the cell structure for tunable waveguide laser upon holographic excitation. (b) Voltage dependence of lasing wavelength in dye-doped NLC waveguide holographically excited.

Fig.20 Schematic explanation of the double PCLC composite film having a twist defect, which is a discontinuity of the director rotation around the helix axis.



of unpolymerized cholesteric LC. This means that the operation wavelength of laser action is thermally stable, which is a great advantage for device application.

4.1.3 Electrically tunable lasing in nematic waveguide under holographic excitation

The distributed feedback (DFB) laser action can be achieved with a transient grating using interference fringes induced by two excitation laser beams (holographic excitation). In this geometry, the lasing wavelength λ_{DFB} upon holographic excitation can be expressed by

$$\lambda_{\text{DFB}} = n_{\text{eff}} \lambda_{\text{ex}} / m \sin \theta,$$

where n_{eff} is the effective refractive index of the active medium, λ_{ex} is the wavelength of excitation beams, m is the order of diffraction, and θ is the half-angle between two excitation beams. According to this equation, the lasing wavelength can be tuned by changing θ and/or n_{eff} . Therefore, if n_{eff} can be electrically controlled, an electrical tuning of laser emission upon holographic excitation can be expected. Based on this concept, we propose an electrical tuning method of the lasing wavelength using a dye-doped NLC as an active laser medium as schematically shown in Fig. 19(a). If LC having extraordinary and ordinary refractive indices, n_e and n_o , is used as the active material for the laser medium, the effective refractive index n_{eff} can be electrically controlled due to the field-induced reorientation of LC molecules. Therefore, when a dye-doped NLC waveguide is holographically excited, the lasing wavelength should be tunable by changing the applied electric field across the LC layer.

Figure 19(b) shows the voltage dependence of the lasing wavelength of the dye-doped NLC waveguide. Above $V=0.8\text{V}$, the lasing peak for the transverse magnetic

(TM)-guided mode (closed circle) showed a continuous red-shift with increasing the applied voltage. The threshold voltage for the peak shift is associated with the Frederiks transition of the NLC. The electrical tuning of laser action could be performed reversibly.

4.2 Photon localization in chiral LCs with defect and its tunability

The localization of the light utilizing the defect mode caused by imperfections in the periodic structure is promising for potential applications such as low threshold lasers and micro-waveguides.⁷⁴⁻⁷⁸⁾

4.2.1 Twist-defect-mode lasing in CLC

Laser actions reported so far in chiral LCs are observed at the edge wavelength of the stop band and are associated with the group velocity anomaly at the photonic band edge. On the other hand, low threshold laser action based on the photon localization at the defect in the periodic structure can also be expected. The introduction of a defect into the periodic helical structure of the CLCs has been theoretically studied.^{79,80)} In particular, Kopp and Genack have predicted the existence of a single circularly polarized localized mode in the twist defect of CLCs.⁸⁰⁾ We experimentally demonstrated the defect mode in the 1-D photonic band gap of the CLC film having a twist defect for the first time. The laser action based on the twist defect mode (TDM) was also observed in dye-doped PCLC composite film

with a twist defect.

The PCLC film with the twist defect was prepared as follows.⁸¹⁾ Photo-polymerizable CLC monomer was spin-coated from a toluene solution onto a glass substrate on which a polyimide (AL-1254) was coated and rubbed in one direction. In order to obtain a uniform planar alignment, the coated CLC was annealed at a temperature just below the clearing point. The CLC molecules on the substrate align their directors parallel to the glass plate, that is, the helical axis is perpendicular to the glass substrate. UV light irradiation was performed using a Xe lamp to induce photopolymerization of the UV-curable CLC monomer. Two PCLC films were put together as the directors of LC molecules at the interface between these films to form a certain angle ϕ . In other words, there is a discontinuous phase jump of the azimuthal angle of the helical structures between these PCLC films at the interface, and it acts as a twist defect in the helicoidal periodic structure, as shown in Fig. 20.

Figure 21(a) shows the transmission spectrum of the dye-doped double-PCLC composite

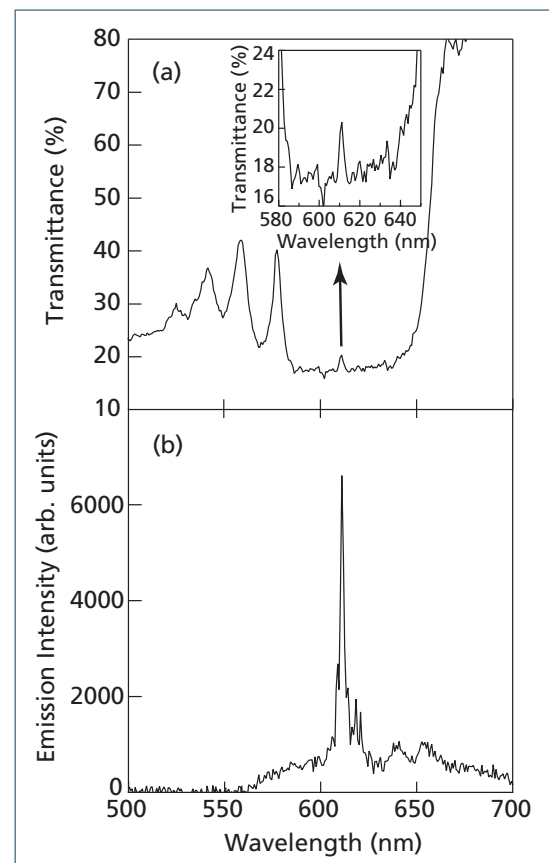


Fig.21 (a) Transmission spectrum of dye-doped double PCLC composite film with twist defect. (b) Emission spectrum of double PCLC composite film at above the threshold pump pulse energy (200 nJ/pulse).

film containing a discontinuous defect interface. A stop band, the 1-D photonic band gap, is confirmed in the spectral range from 580 to 640 nm. It should be noted that a sharp peak appears at 611 nm within the photonic band gap, which might be related to the defect mode induced by the introduction of the twist defect interface.

Figure 21(b) shows the emission spectrum of the dye-doped double-PCLC composite film with the defect interface at the pump energy of 200 nJ/pulse. At a high excitation energy (200 nJ/pulse), laser action appears at 611 nm, which is within the band gap and coincides with the TDM wavelength. With increasing excitation energy, another sharp emission peak appears at 638 nm which, corresponds to the edge wavelength of the stop band. This emission peak might be associated with the band-edge lasing that appears in PCLC without any defect. Consequently, defect-mode lasing occurs at a lower pumping energy compared with that of band-edge lasing.

4.2.2 Transient defect mode induced by partial deformation of helix

The TDM based on the composite film of two PCLCs has been achieved. However, its wavelength cannot be tuned by applying an external field such as an electric field or light. We have proposed a new type of defect mode in the helix, that can be dynamically tuned by applying an external field.⁸²⁾ Figure 22 shows a schematic explanation of a photonic defect in CLC. If the periodicity (pitch) of the helix is partially changed, that is, the pitch is partially squeezed or expanded, these irregularities in the periodic structure should act as defects

and cause light localization. As a method of inducing partial change in the helix pitch, we propose that the local modification of helical twisting power (HTP) induced by irradiation with focused Gaussian laser light. Optical control of HTP can be realized by using the photochemical effects of the doped azobenzene, nonlinear optical effects, or simply by heating. Photoinduced reversible control of the HTP of CLC has been demonstrated in CLC containing photochromic azobenzene, and applications to reflection display devices, optical shutters, and optical memory, for example, have been studied.^{83,84)} By *trans-cis* photoisomerization of the doped azobenzene, the HTP of the host CLC changes, so that photoinduced control of HTP can be realized.

Figure 23 shows the calculated transmission spectra for the right-handed circularly polarized (RCP) and left-handed circularly polarized (LCP) light passing through the CLC with a chiral-defect-induced partial helix deformation. The calculation was carried out assuming that the HTP is modulated as $HTP(z) = HTP_0[1 + \alpha \exp(-2z^2/w^2)]$, where the z -axis is parallel to the helix axis and $2w$ is the diameter of the light beam, α is the modulation strength of HTP, and HTP_0 is the initial HTP. The helix sense of CLC is right-handed. The pitch of the helix is 350 nm, and ordinary and extraordinary refractive indices of LC are 1.5 and 1.7, respectively. The thickness of the CLC is 5 μ m. A transmission peak based on the defect mode was observed in the stop band for the RCP light. On the other hand, when the incident light was LCP, no defect mode was observed. In other words, the defect mode due to the photon localization in our system can be realized only for the

circularly polarized light with the same handedness as the helix, which is similar to the result for the TDM. The position of the defect mode depends on α and w . With decreasing α , a transmission peak due to the defect mode shifts towards the longer-wavelength edge. On the contrary, with increasing α , the peak shifts towards the shorter-wavelength edge. The increase and decrease in α correspond to the squeezing and expansion of the helix pitch. Therefore, the tuning of defect modes could be achieved by partial squeezing and expansion of the helix.

4.2.3 Chiral defect fabricated by direct laser writing technique

We have proposed a novel approach to introducing chiral defects (local modulation of the helix pitch) into the helix structure of CLC.^{85,86)} A schematic explanation of the fabrication procedure is shown in Fig. 24(a). A 100 fs pulse of a Ti:sapphire laser at the wavelength of 800 nm and repetition rate of 80 MHz was focused on the sample cell through an objective lens with numerical aperture (NA) 1.4. A right-handed PCLC material doped with 1 wt% of DCM dye aligned homogeneously in a cell with a gap of 6–7 μ m. Direct laser writing was performed with a confocal laser scanning microscope. The laser was scanned over an area of 146.2 \times 146.2 μ m², with a scan-line resolution of 2048 lines per scan area. First, the laser light was tightly focused near the substrate surface in the CLC cell. Two-photon polymerization occurred at the laser focal point and a locally polymerized PCLC thin film was obtained on the substrate surface. The sample was then flipped over and laser writing was performed

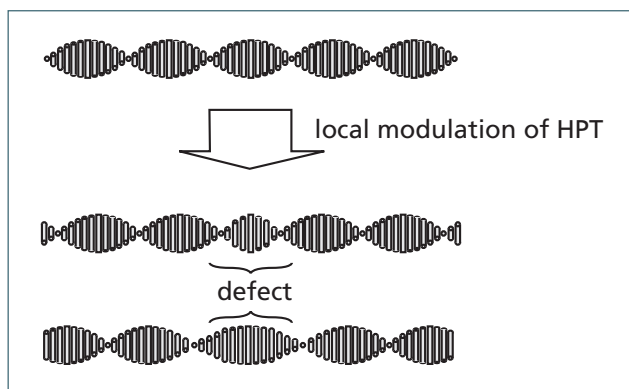


Fig.22 Schematic explanation of the optically induced chiral defect based on the partial deformation of the helix pitch.

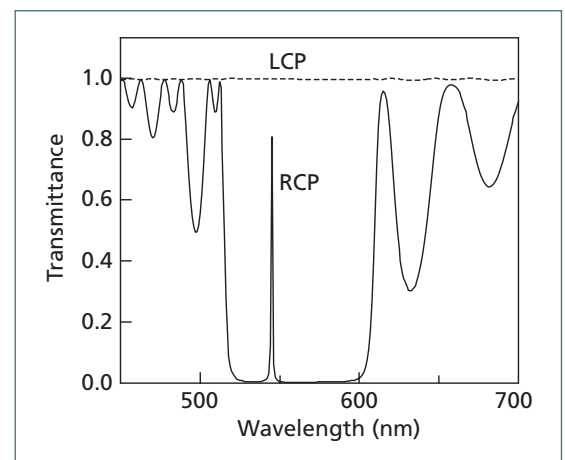


Fig.23 Transmission spectra of RCP and LCP light passing through the CLC with deformation-induced chiral defect ($\alpha = -0.2$, $w = 300$ nm).

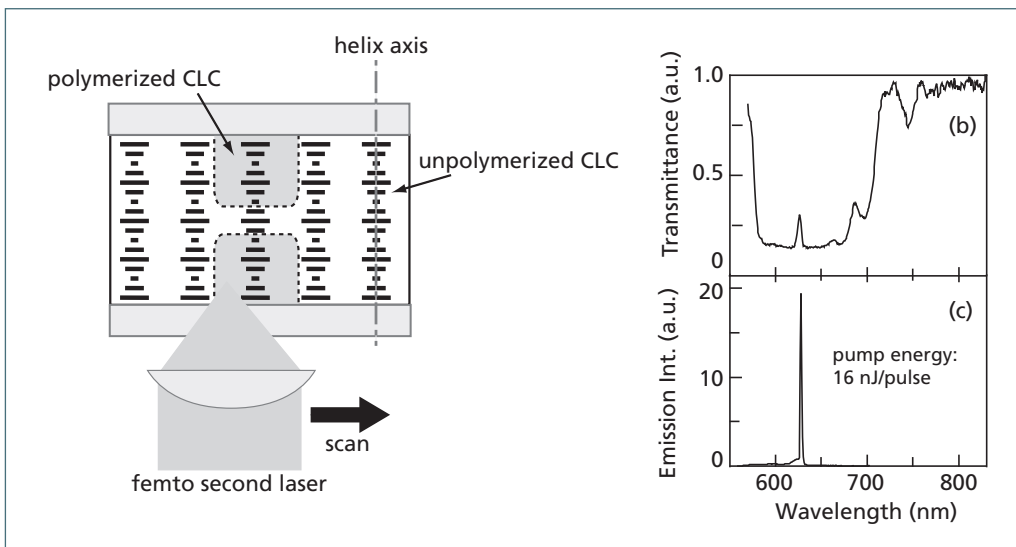


Fig.24 (a) Schematic explanation of fabrication procedure of PCLC with chiral defect based on local photopolymerization using scanning confocal microscope. (b) Transmission and (c) emission spectra of CLC with chiral defect.

again near the opposite surface of the cell. As a result, a hybrid structure was fabricated, in which an unpolymerized CLC region remained between two PCLC films on the cell surface.

Figure 24(b) shows the transmission spectra for right-handed circularly polarized light of the fabricated CLC defect structure. A single-defect mode is observed within the selective reflection band of the CLC. The theoretical transmission spectrum was calculated using Berreman's 4×4 matrix, and good agreement with the experimental result was obtained. Figure 19(c) shows the emission spectrum of the CLC single-defect structure at high pumping energy, along with the corresponding transmission spectrum. Single-mode laser action is observed at 628 nm, which corresponds to the defect-mode wavelength. The lasing threshold for the defect mode structure is 16.7 mJ/cm^2 , which is less than half the threshold in CLC without the defect structure. The reduction of the lasing threshold in the defect structure is evidence of a high-Q cavity formed by the defect.

5. Tunable-Defect-Mode Lasing in Periodic Structure Containing LC Layer as Defect

LCs have high optical anisotropy and are sensitive to external stress such as an electric field. On the basis of such optical anisotropy and field sensitivity, a TPC has been proposed in opal or inverse opal infiltrated with LC.⁸⁷⁻⁹¹ Although opal and inverse opal are simple and inexpensive means of realizing 3-D PCs by self-organization of colloidal particles,^{92,93} the introduction of defects into the 3-D periodic

structure is a problem that must be resolved. Not only 3-D PCs but also 1-D PCs are attractive subjects. Although, the 1-D PC does not have a complete PBG, there are numerous applications using the extraordinary dispersion of the photon and localized photonic state in a defect layer. So far, intensive studies on 1-D PC applications have been reported: air-bridge microcavities,⁹⁴ photonic band-edge lasers,⁹⁵ nonlinear optical diodes,⁹⁶ and the enhancement of optical nonlinearity.^{77,97,98} Recently we introduced a LC layer in a dielectric multilayer structure as a defect in 1-D PC,⁹⁹ in which the wavelength of defect modes was controlled by applying electric field because of a change in the optical length of the defect layer caused by the field-induced molecular reorientation of LC.

5.1 Tunable-defect-mode lasing in periodic structure containing LC layer as defect

We have introduced a LC layer in a 1-D PC as a defect, where the wavelength of defect modes was controlled by applying electric field because of a change in the optical length of the defect layer caused by the field-induced molecular reorientation of LC.¹⁰⁰ We also proposed a wavelength-tunable laser based on an electrically controllable defect mode in a 1-D dielectric periodic structure containing a dye-doped LC as a defect layer.^{101,102} Figure 25 shows the 1-D PC with a LC defect. A dielectric multilayer consisting of stack of alternating SiO_2 and TiO_2 layers deposited on an ITO-coated glass substrate is used as the 1-D PC. In order

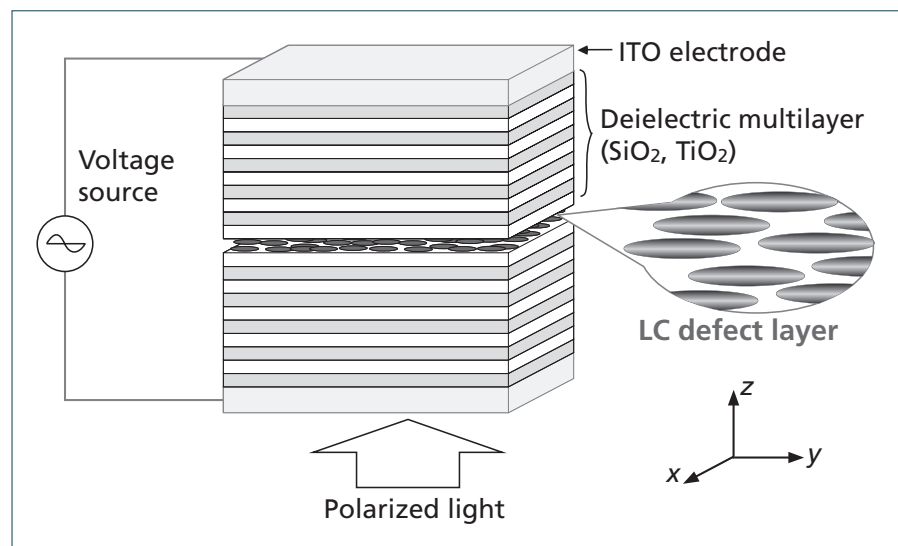


Fig.25 Schematic explanation of 1-D PC containing liquid crystal as defect.

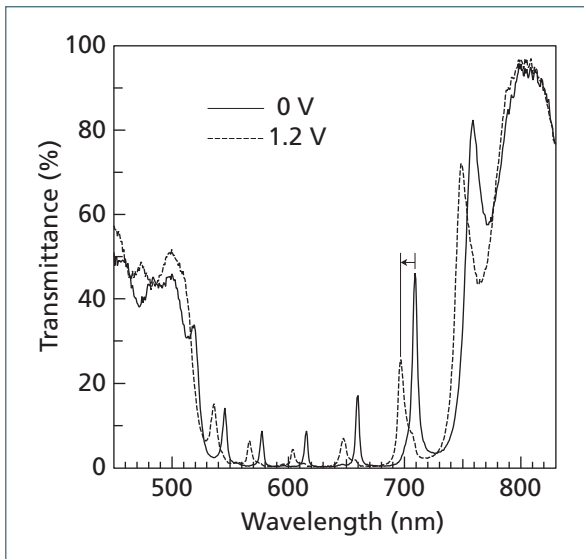


Fig.26 Transmission spectra of 1-D PC with LC defect as a function of applied voltage.

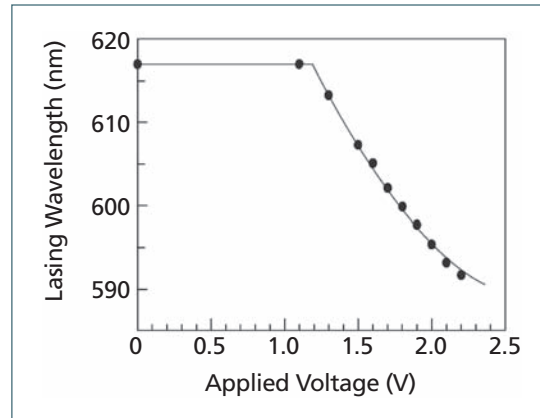


Fig.27 Voltage dependence of defect-mode lasing wavelength in the 1-D PC with dye-doped NLC defect.

to introduce the defect layer, a dye-doped NLC (Merck E47) was sandwiched between substrates with dielectric multilayers using $2\mu\text{m}$ spacers. The refractive index anisotropy Δn of E47 is 0.209 at RT. In the absence of an elec-

tric field, the long molecular axis of the LC is aligned parallel to the substrates (y -axis).

In order to investigate the characteristics of the defect mode, the transmission spectrum of the linearly polarized light propagating along the z -axis was measured from the opposite side of the cell using a charge-coupled device (CCD) multichannel spectrometer.

Figure 26 shows the voltage dependence of transmission spectra for incident light polarized along the y -axis, which corresponds to the rubbing direction and the initial orientation direction of the LC molecules in the defect layer, as shown in Fig. 25. A rectangular wave voltage of 1 kHz was applied between ITO layers to change the molecular alignment of the LC in the defect layer. The solid and dashed lines correspond to spectra at 0 and 1.2 V, respectively. The peaks of the defect modes shift to shorter wavelengths upon applying voltage. This peak shift originates from the decrease in the optical length of the defect layer caused by the field-induced reorienta-

tion of the LC molecules. Consequently, we confirmed that the wavelength of the defect mode in a 1-D PC with the LC layer as a defect can be controlled by applying voltage.

On the basis of the above-described defect-mode tuning, the lasing wavelength can be controlled by applying electric field.^{101,102} Figure 27 shows the voltage dependence of the lasing peak wavelength in a 1-D PC with DCM-doped LC. The lasing peak shifts toward shorter wavelengths with increasing voltage, in the same manner as the defect mode shift shown in Fig. 26. The wavelength shift of the lasing peak is about 25 nm, even upon applying low voltage. As is evident from Fig. 27, a threshold voltage exists for the peak shift, and the lasing wavelength shifts towards shorter wavelengths above the threshold of 1.1 V. This is associated with Frederiks transition of the LC in the defect layer.

5.2 Double periodic structure: Helix defect in 1-D PC

We have also introduced a CLC layer in a 1-D PC as a defect.¹⁰³⁻¹⁰⁵ Figure 28(a) shows the theoretical transmission spectrum of a 10-pair multilayer without a CLC defect (solid line), and a simple CLC without a PC structure (dashed line). The PBG of the CLC was observed between 605 and 680 nm, which is within the PBG of the multilayer. Figure 28(b) shows the calculated transmission spectrum of a 1-D HPC with a CLC defect. Many peaks appear at regular intervals in the PBG

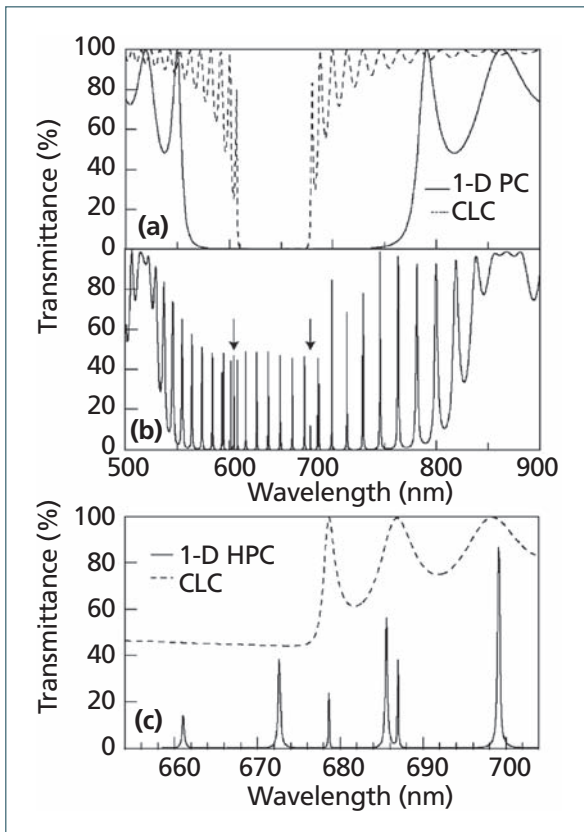


Fig.28 (a) Theoretical transmission spectra of 1-D PC without any defect (solid line) and CLC without PC structure (dashed line). (b) Theoretical transmission spectra of 1-D PC containing CLC as a defect. (c) Magnified transmission spectra corresponding to (b).

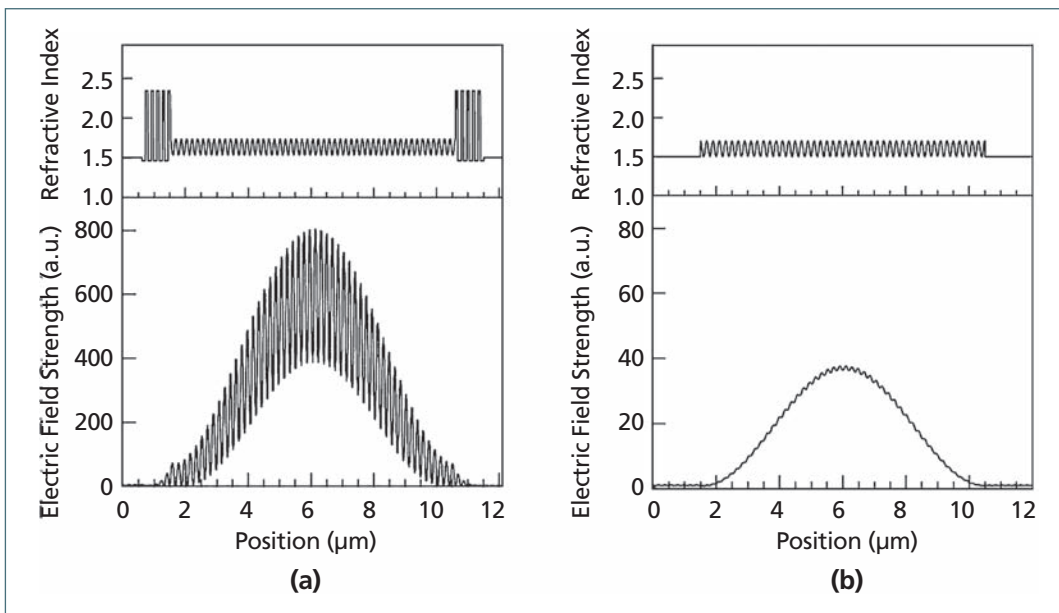


Fig.29 Calculated electric field strength in the cell of (a) 1-D PC containing CLC defect and (b) simple CLC.

of the HPC. These peaks are related to the defect modes resulting from the introduction of the CLC defect. However, additional peaks were observed, as indicated by arrows, which disrupted the regular interval between the defect-mode peaks at both band edges of the CLC.

The transmission spectra in Fig. 28(b), magnified around the longer edge of the PBG of the CLC, are shown in Fig. 28(c). Four main peaks due to the defect modes appear at regular intervals (661, 673, 687, and 699 nm), although the peak at 687 nm splits. This splitting is attributed to the optical anisotropy of the CLC. Therefore, two kinds of defect modes corresponding to left- and right-handed circularly polarized light could exist outside the PBG of the CLC. On the other hand, one additional peak was observed at 678.6 nm, which corresponds to the band-edge wavelength of the CLC. By detailed consideration of the polarization states of transmitted light, the additional peak was clearly distinguished from the other defect mode peaks. Such a peak was not observed in a 1-D PC with a uniform defect, such as an isotropic medium or nematic LCs.^{100,106} Namely, this peak is a defect mode peculiar to the helix defect in the 1-D PC, and is associated with photon localization originating from the band-edge effect of the CLC helix. Note that this defect mode peak is very sharp and the FWHM of this peak is 0.05 nm, which is more than four times smaller than that of other defect-mode peaks (0.23 nm). From the peak width, the Q -factor of the

additional mode at the band edge of the CLC was estimated to be 14000, which was much higher than those of the other defect modes.

In order to clarify the appearance of the high- Q defect mode in the double-periodic structure, we have performed a theoretical estimation of the electric field distribution in the three types of 1-D periodic structures described above, by a finite difference time domain (FDTD) method. Figure 29 shows the calculated electric field distributions and refractive indices in two types of periodic structures. The wavelength of the incident light to the periodic structures corresponds to the high- Q defect mode wavelength. It should be noted that light is strongly localized in the double-periodic structure and the maximum electric field intensity is more than 15 times as much as that of a simple CLC. Light is localized at the center of the CLC layer in the double periodic structure shown in Fig. 29(a) and its field pattern is similar to that in the CLC shown in Fig. 29(b), which indicates that light in the double-periodic structure is confined by the band-edge effect of CLC. Additionally, light confinement is effectively enhanced by the outer periodic structure because the wavelength of light is within the PBG of the outer periodic structure. Namely, because of the

contributions of both the band-edge effect of CLC and the defect-mode effect of the outer periodic structure, light is strongly localized in the double-periodic structure.

We have investigated the laser action in a 1-D HPC with a CLC defect. At a high pumping energy of 18 nJ/pulse, as shown in Fig. 30(a), only one sharp lasing peak appears at 643.5 nm. The calculated transmission spectrum of this system is also shown in Fig. 30(b). Upon comparing Figs. 30(a) and 30(b), the lasing peak is seen to coincide with the wavelength of the peculiar defect mode. Note

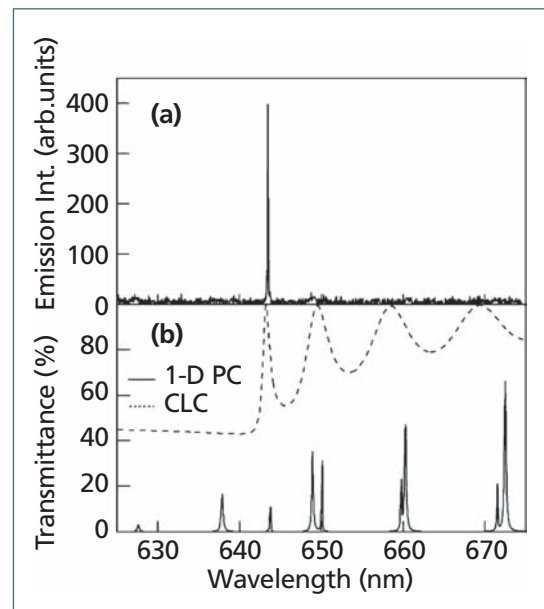


Fig.30 (a) Emission spectrum of 1-D PC-containing dye-doped CLC defect layer. (b) Theoretical transmission spectra corresponding to the emission spectrum.

that the laser action was a single mode based on one additional mode, although many modes exist because of the high Q -factor. The threshold of laser action in the 1-D HPC with a CLC defect was lower than that in simple CLC without a 1-D PC.¹⁰³⁾ This result is attributed to the strong optical confinement due to the high Q -factor of the additional mode. Similar results have been confirmed in the 1-D PC containing FLC as a defect.¹⁰⁷⁾

6. Tunable Two-Dimensional Photonic Crystal

Various types of two-dimensional (2-D) PCs have been studied.¹⁰⁸⁻¹¹¹⁾ In 2-D PCs, the

PBG and defect states also play important roles. We are interested in the characteristics of photons in waveguides in 2-D PCs.

With a Y-shaped waveguide in LC-infiltrated 2-D PCs, switching of the light propagation direction and its temporal behavior have been theoretically clarified. Details are now under study.

7. Summary

In this article, the historical background and recent progress in organic electronics and photonic crystals have been discussed. Novel characteristics of organic electronic devices mainly utilizing conducting polymers and related

with optical effects and tunable photonic crystals composed of a periodic structure of optical-wavelength order combined with functional organic materials have been demonstrated.

These new devices exhibit tremendous novel characteristics, with which various new applications will be developed. We are convinced that these organic electronic devices and photonic crystals will become the key technology in sustaining the 21st century.

It should also be noted that these devices are also important from environmental viewpoints.

JSAP

- 1) H. Akamatu, H. Inokuchi, and Y. Matsunaga: *Nature* **173** (1954) 168.
- 2) R. L. Greene, G. B. Street, and L. J. Suter: *Phys. Rev. Lett.* **35** (1975) 577.
- 3) C. K. Chiang, C. R. Fincher, Jr., Y. W. Park, A. J. Heeger, H. Shirakawa, E. J. Louis, S. C. Gau, and A. G. MacDiarmid: *Phys. Rev. Lett.* **39** (1977) 1098.
- 4) T. R. Hebner, C. C. Wu, D. Marcy, M. H. Lu, and J. C. Strum: *Appl. Phys. Lett.* **72** (1998) 519.
- 5) R. Sugimoto, S. Takeda, H. B. Gu, and K. Yoshino: *Chem. Express* **1** (1986) 635.
- 6) K. Yoshino, S. Nakajima, D. H. Park, and R. Sugimoto: *Jpn. J. Appl. Phys.* **27** (1988) L716.
- 7) K. Yoshino, Y. Manda, K. Sawada, M. Onoda, and R. Sugimoto: *Solid State Commun.* **69** (1989) 143.
- 8) M. Fukuda, K. Sawada, and K. Yoshino: *Jpn. J. Appl. Phys.* **28** (1989) L1433.
- 9) Y. Ohmori, M. Uchida, K. Muro, and K. Yoshino: *Jpn. J. Appl. Phys.* **30** (1991) L1941.
- 10) Y. Ohmori, M. Uchida, K. Muro, and K. Yoshino: *Jpn. J. Appl. Phys.* **30** (1991) L1938.
- 11) M. Hamaguchi and K. Yoshino: *Appl. Phys. Lett.* **69** (1996) 143.
- 12) M. Hamaguchi and K. Yoshino: *Appl. Phys. Lett.* **67** (1995) 3381.
- 13) Y. Yoshida, Y. Nishihara, R. Ootake, A. Fujii, M. Ozaki, K. Yoshino, H. K. Kim, N. S. Baek, and S. K. Choi: *J. Appl. Phys.* **90** (2001) 6061.
- 14) Y. Yoshida, Y. Nishihara, A. Fujii, M. Ozaki, K. Yoshino, H. K. Kim, N. S. Baek, and S. K. Choi: *J. Appl. Phys.* **95** (2004) 4193.
- 15) A. Fujii, R. Ootake, T. Fujisawa, M. Ozaki, Y. Ohmori, T. Laga, H.-F. Lu, H. S. O. Chan, S.-C. Ng, and K. Yoshino: *Appl. Phys. Lett.* **77** (2000) 660.
- 16) S. C. Ng, H. F. Lu, H. S. O. Chan, A. Fujii, T. Laga, and K. Yoshino: *Macromolecules* **34** (2001) 6895.
- 17) D. F. O'Brien, M. A. Baldo, M. E. Thompson, and S. R. Forrest: *Appl. Phys. Lett.* **74** (1999) 442.
- 18) M. A. Baldo, S. Lamansky, P. E. Burrows, M. E. Thompson, and S. R. Forrest: *Appl. Phys. Lett.* **75** (1999) 4.
- 19) Y. Hino, H. Kajii, and Y. Ohmori: *Jpn. J. Appl. Phys.* **43** (2004) 2315.
- 20) Y. Hino, H. Kajii, and Y. Ohmori: *IEICE Trans. Electron.* **E87-C** (2004) 2053.
- 21) C. Adachi, M. A. Baldo, M. E. Thompson, and S. R. Forrest: *J. Appl. Phys.* **90** (2001) 5048.
- 22) Y. Hino, H. Kajii, and Y. Ohmori: *Org. Electron.* **5** (2004) 265.
- 23) Y. Hino, H. Kajii, and Y. Ohmori: *Jpn. J. Appl. Phys.* **44** (2005) 2790.
- 24) Y. Ohmori, H. Kajii, M. Kaneko, K. Yoshino, M. Ozaki, A. Fujii, M. Hikita, and H. Takenaka: *IEEE J. Sel. Top. Quantum Electron.* **10** (2004) 70.
- 25) S. V. Frolov, M. Shkunov, Z. V. Vardeny, and K. Yoshino: *Phys. Rev. B* **56** (1997) R4363.
- 26) S. V. Frolov, M. Ozaki, W. Gellermann, Z. V. Vardeny, and K. Yoshino: *Jpn. J. Appl. Phys.* **35** (1996) L1371.
- 27) S. V. Frolov, Z. V. Vardeny, and K. Yoshino: *Appl. Phys. Lett.* **72** (1998) 1802.
- 28) S. V. Frolov, A. Fujii, D. Chinn, K. Yoshino, and Z. V. Vardeny: *Appl. Phys. Lett.* **72** (1998) 2811.
- 29) S. V. Frolov, A. Fujii, D. Chinn, M. Hirohata, R. Hidayat, M. Teraguchi, T. Masuda, K. Yoshino, and Z. V. Vardeny: *Adv. Mater.* **10** (1998) 869.
- 30) Y. Yoshida, T. Nishimura, A. Fujii, M. Ozaki, and K. Yoshino: *Appl. Phys. Lett.* **86** (2005) 141903.
- 31) B. O'Regan and M. Gratzel: *Nature* **353** (1991) 737.
- 32) S. Morita, A. A. Zakhidov, and K. Yoshino: *Solid State Commun.* **82** (1992) 249.
- 33) K. Yoshino, S. Morita, and A. A. Zakhidov: *Chem. Express* **7** (1992) 817.
- 34) K. Yoshino, X. H. Yin, S. Morita, T. Kawai, and A. A. Zakhidov: *Solid State Commun.* **85** (1993) 85.
- 35) S. Morita, A. A. Zakhidov, and K. Yoshino: *Jpn. J. Appl. Phys.* **32** (1993) L873.
- 36) K. Yoshino, K. Tada, A. Fujii, E. M. Conwell, and A. A. Zakhidov: *IEEE Trans. Electron Devices* **44** (1997) 1315.
- 37) K. Yoshino, S. Lee, A. Fujii, H. Nakayama, W. Schneider, A. Naka, and M. Ishikawa: *Adv. Mater.* **11** (1999) 1382.
- 38) T. Umeda, T. Shirakawa, A. Fujii, and K. Yoshino: *Jpn. J. Appl. Phys.* **42** (2003) L1475.
- 39) T. Shirakawa, T. Umeda, Y. Hashimoto, A. Fujii, and K. Yoshino: *J. Phys. D* **37** (2004) 847.
- 40) T. Umeda, H. Noda, T. Shibata, A. Fujii, K. Yoshino, and M. Ozaki: *Jpn. J. Appl. Phys.* **45** (2006) 5241.
- 41) H. Koezuka, K. Hyodo, and A. G. MacDiarmid: *J. Appl. Phys.* **58** (1985) 1279.
- 42) K. Kaneto, S. Takeda, and K. Yoshino: *Jpn. J. Appl. Phys.* **24** (1985) L553.

- 43) S. Takeda, K. Kaneto, and K. Yoshino: Chem. Express **1** (1986) 383.
- 44) H. Kajii, H. Okuya, A. Sakakibara, and Y. Ohmori: Jpn. J. Appl. Phys. **44** (2005) L1567.
- 45) K. Yoshino, K. Kaneto, and Y. Inuishi: Jpn. J. Appl. Phys. **22** (1983) L157.
- 46) K. Kaneto, K. Yoshino, and Y. Inuishi: Jpn. J. Appl. Phys. **22** (1983) L412.
- 47) K. Kaneto, H. Agawa, and K. Yoshino: J. Appl. Phys. **61** (1987) 1197.
- 48) W. Lu, A. G. Fadeev, B. Qi, E. Smela, B. R. Mattes, J. Ding, G. M. Spinks, J. Mazurkiewics, D. Zhou, G. G. Wallace, D. R. MacFarlane, S. A. Forsyth, and M. Forsyth: Science **297** (2002) 983.
- 49) E. Yablonovitch: Phys. Rev. Lett. **58** (1987) 2059.
- 50) S. John: Phys. Rev. Lett. **58** (1987) 2486.
- 51) J. D. Joannopoulos, R. D. Meade, and J. N. Winn: *Photonic Crystals: Molding the Flow of Light* (Princeton Univ. Press, Princeton, NJ, 1995).
- 52) J. Martorell and N. M. Lawandy: Phys. Rev. Lett. **65** (1990) 1877.
- 53) K. Yoshino, S. B. Lee, S. Tatsuhara, Y. Kawagishi, M. Ozaki, and A. A. Zakhidov: Appl. Phys. Lett. **73** (1998) 3506.
- 54) K. Yoshino, S. Tatsuhara, Y. Kawagishi, M. Ozaki, A. A. Zakhidov, and Z. V. Vardeny: Appl. Phys. Lett. **74** (1999) 2590.
- 55) J. S. Foresi, P. R. Villeneuve, J. Ferrera, E. R. Thoen, G. Steinmeyer, S. Fan, J. D. Joannopoulos, L. C. Kimerling, H. I. Smith, and E. P. Ippen: Nature **390** (1997) 143.
- 56) O. Painter, R. K. Lee, A. Scherer, A. Yariv, J. D. O'Brien, P. D. Dapkus, and I. Kim: Science **284** (1999) 1819.
- 57) S. Noda, K. Tomoda, N. Yamamoto, and A. Chutinan: Science **289** (2000) 604.
- 58) K. Yoshino, K. Tada, M. Ozaki, A. A. Zakhidov, and R. H. Baughman: Jpn. J. Appl. Phys. **36** (1997) L714.
- 59) Y. A. Vlasov, K. Luterova, I. Pelant, B. Honerlage, and V. N. Astratov: Appl. Phys. Lett. **71** (1997) 1616.
- 60) A. A. Zakhidov, R. H. Baughman, Z. Iqbal, C. Cui, I. Khayrullin, S. O. Dantas, J. Marti, and V. G. Ralchenko: Science **282** (1998) 290.
- 61) K. Yoshino: unpublished.
- 62) K. Yoshino, R. Ozaki, J. Matsumoto, M. Ojima, S. Hiwatashi, Y. Matsuhisa, and M. Ozaki: IEEE Trans. Dielectr. Electr. Insul. **13** (2006) 678.
- 63) S. Chandrasekhar: *Liquid Crystals* (Cambridge University Press, Cambridge, U.K., 1992).
- 64) V. I. Kopp, B. Fan, H. K. Vithana, and A. Z. Genack: Opt. Lett. **23** (1998) 1707.
- 65) K. Funamoto, M. Ozaki, and K. Yoshino: Jpn. J. Appl. Phys. **42** (2003) L1523.
- 66) M. Ozaki, M. Kasano, D. Ganzke, W. Haase, and K. Yoshino: Adv. Mater. **14** (2002) 306.
- 67) M. Ozaki, M. Kasano, D. Ganzke, W. Haase, and K. Yoshino: Adv. Mater. **15** (2003) 974.
- 68) M. Kasano, M. Ozaki, D. Ganzke, W. Haase, and K. Yoshino: Appl. Phys. Lett. **82** (2003) 4026.
- 69) H. Finkelmann, S. T. Kim, A. Munoz, P. Palffy-Muhoray, and B. Taheri: Adv. Mater. **13** (2001) 1069.
- 70) T. Matsui, R. Ozaki, K. Funamoto, M. Ozaki, and K. Yoshino: Appl. Phys. Lett. **81** (2002) 3741.
- 71) J. P. Dowling, M. Scalora, M. J. Bloemer, and C. M. Bowden: J. Appl. Phys. **75** (1994) 1896.
- 72) J. W. Goodby, R. Blinc, N. A. Clark, S. T. Lagerwall, M. A. Osipov, S. A. Pikin, T. Sakurai, K. Yoshino, and B. Zeks: *Ferroelectric Liquid Crystals* (Gordon and Breach Science, Philadelphia, PA, 1991).
- 73) K. Hori: Mol. Cryst. Liq. Cryst. **82** (1982) L13.
- 74) J. S. Foresi, P. R. Villeneuve, J. Ferrera, E. R. Thoen, G. Steinmeyer, S. Fan, J. D. Joannopoulos, L. C. Kimerling, H. I. Smith, and E. P. Ippen: Nature **390** (1997) 143.
- 75) O. Painter, R. K. Lee, A. Scherer, A. Yariv, J. D. O'Brien, P. D. Dapkus, and I. Kim: Science **284** (1999) 1819.
- 76) S. Noda, K. Tomoda, N. Yamamoto, and A. Chutinan: Science **289** (2000) 604.
- 77) T. Hattori, N. Tsurumachi, and H. Nakatsuka: J. Opt. Soc. Am. B **14** (1997) 348.
- 78) R. Ozaki, T. Matsui, M. Ozaki, and K. Yoshino: Jpn. J. Appl. Phys. **41** (2002) L1482.
- 79) Y. C. Yang, C. S. Kee, J. E. Kim, H. Y. Park, J. C. Lee, and Y. J. Jeon: Phys. Rev. E **60** (1999) 6852.
- 80) V. I. Kopp and A. Z. Genack: Phys. Rev. Lett. **89** (2002) 033901.
- 81) M. Ozaki, R. Ozaki, T. Matsui, and K. Yoshino: Jpn. J. Appl. Phys. **42** (2003) L472.
- 82) T. Matsui, M. Ozaki, and K. Yoshino: Phys. Rev. E **69** (2004) 061715.
- 83) E. Sackmann: J. Am. Chem. Soc. **93** (1971) 7088.
- 84) H. K. Lee, K. Doi, H. Harada, O. Tsutsumi, A. Kanazawa, T. Shiono, and T. Ikeda: J. Phys. Chem. B **104** (2000) 7023.
- 85) H. Yoshida, C. H. Lee, Y. Matsuhisa, A. Fujii, and M. Ozaki: to be published in Adv. Mater.
- 86) H. Yoshida, C. H. Lee, A. Fujii, and M. Ozaki: Appl. Phys. Lett. **89** (2006) 231913.
- 87) K. Yoshino, S. Satoh, Y. Shimoda, Y. Kawagishi, K. Nakayama, and M. Ozaki: Jpn. J. Appl. Phys. **38** (1999) L961.
- 88) K. Yoshino, Y. Shimoda, Y. Kawagishi, K. Nakayama, and M. Ozaki: Appl. Phys. Lett. **75** (1999) 932.
- 89) K. Busch and S. John: Phys. Rev. Lett. **83** (1999) 967.
- 90) Y. Shimoda, M. Ozaki, and K. Yoshino: Appl. Phys. Lett. **79** (2001) 3627.
- 91) M. Ozaki, Y. Shimoda, M. Kasano, and K. Yoshino: Adv. Mater. **14** (2002) 514.
- 92) K. Yoshino, K. Tada, M. Ozaki, A. A. Zakhidov, and R. H. Baughman: Jpn. J. Appl. Phys. **36** (1997) L714.
- 93) Y. A. Vlasov, K. Luterova, I. Pelant, B. Honerlage, and V. N. Astratov: Appl. Phys. Lett. **71** (1997) 1616.
- 94) J. S. Foresi, P. R. Villeneuve, J. Ferrera, E. R. Thoen, G. Steinmeyer, S. Fan, J. D. Joannopoulos, L. C. Kimerling, H. I. Smith, and E. P. Ippen: Nature **390** (1997) 143.
- 95) J. P. Dowling, M. Scalora, M. J. Bloemer, and C. M. Bowden: J. Appl. Phys. **75** (1994) 1896.
- 96) M. D. Tocci, C. M. Bloemer, M. Scalora, J. P. Dowling, and C. M. Bowden: Appl. Phys. Lett. **66** (1995) 2324.
- 97) K. Yoshino: J. Soc. Elect. Mat. Eng. **9** (2000) 101.
- 98) Y. Dumeige, P. Vidakovic, S. Sauvage, I. Sgnes, and J. A. Levenson: Appl. Phys. Lett. **78** (2001) 3021.
- 99) R. Ozaki, T. Matsui, M. Ozaki, and K. Yoshino: Jpn. J. Appl. Phys. **41** (2002) L1482.
- 100) R. Ozaki, T. Matsui, M. Ozaki, and K. Yoshino: Jpn. J. Appl. Phys. **41** (2002) L1482.
- 101) R. Ozaki, T. Matsui, M. Ozaki, and K. Yoshino: Appl. Phys. Lett. **82** (2003) 3593.
- 102) R. Ozaki, Y. Matsuhisa, M. Ozaki, and K. Yoshino: Appl. Phys. Lett. **84** (2004) 1844.
- 103) Y. Matsuhisa, R. Ozaki, M. Ozaki, and K. Yoshino: Jpn. J. Appl. Phys. **44** (2005) L629.
- 104) Y. Matsuhisa, R. Ozaki, K. Yoshino, and M. Ozaki: Appl. Phys. Lett. **89** (2006) 101109.
- 105) Y. Matsuhisa, R. Ozaki, K. Yoshino, and M. Ozaki: Thin Solid Films **509** (2006) 189.
- 106) R. Ozaki, T. Sanda, H. Yoshida, Y. Matsuhisa, M. Ozaki, and K. Yoshino: Jpn. J. Appl. Phys. **45** (2006) L493.
- 107) Y. Matsuhisa, W. Haase, A. Fujii, and M. Ozaki: Appl. Phys. Lett. **89** (2006) 201112.
- 108) H. Takeda and K. Yoshino: J. Appl. Phys. **92** (2002) 5658.
- 109) H. Takeda and K. Yoshino: Phys. Rev. B **67** (2003) 073106.
- 110) H. Takeda and K. Yoshino: Phys. Rev. E **67** (2003) 056607.
- 111) H. Takeda and K. Yoshino: Phys. Rev. E **70** (2004) 026601.



Katsumi Yoshino was born in Shimane Japan in 1941. He graduated in 1964 from Department of Electrical Engineering, Faculty of Engineering, Osaka University, where he received Ph. D. degree. In 1969 he became a research associate at the Department of Electrical

Engineering, Osaka University, and in 1972, he was promoted to an Assistant Professor in 1972, to an Associate Professor in 1978 and to Full Professor in 1988. From 1974 to 1975 he was a visiting scientist at the Hahn-Meitner Institut für Kernforschung in Berlin. From 2005, he has been a Professor of Emeritus of Osaka University. He has been also a professor of Shimane University and Nagasaki Institute of Applied Science and an Advisor of Shimane Institute for Industrial Technology. From 2007 he has been an Director General of Shimane Institute for Industrial Technology.

He was the vice president of the Institute of Electrical Engineers of Japan and the president of the Japanese Liquid Crystal Society. He received the Applied Physics Award (1984), Osaka Scientific Award (1990), Book of Year Award (1997) and Outstanding Achievement Award from The Institute of Electrical Engineers of Japan (1998), Fellow from The Institute of Electronics, Information and Communication Engineers (2001), The Best Paper Award from the Society of Electrical Material Engineering (2001), the Best Paper Award from The Japanese Liquid Crystal Society (2002), Japanese Liquid Crystal Society Award (2003), Fellow from IEEE (2004), The Best Paper Award from Japanese Institute of Electrical Engineer (2004) and The Contribution Award for Polymer Science from the Society of Polymer Science, Japan.



Yutaka Ohmori graduated in 1972 from Department of Electrical Engineering, Faculty of Engineering, Osaka University, Osaka, Japan, where he received the Doctor of Engineering degree. In 1977, he joined Nippon Telegraph Telephone Public Corporation (now

NTT Corporation), where he worked mainly research on optical semiconductor devices. In 1989, he became an associate professor in Electrical Engineering, Faculty of Engineering, Osaka University. In 2000, he became a professor in Collaborative Research Center for Advanced Science and Technology, Electronic Materials and Systems Engineering, Osaka University, and now he is a professor of Center for Advanced Science and Innovation (CASI), where he worked on optical and electrical devices utilizing organic materials including conducting polymers. Professor Ohmori is a fellow of the Institute of Electrical and Electronics Engineers, Inc. (IEEE), and a member of the Japan Society of Applied Physics (JSAP), the Institute of Electronics, Information and Communication Engineers (IEICE), American Physical Society (APS), The International Society for Optical Engineering (SPIE), and the Materials Research Society (MRS).



Masanori Ozaki received his B.E., M.E., and D.E. degrees from Osaka University in 1983, 1995, and 1988, respectively. He joined Department of Electronic Engineering in Osaka University as a research associate in 1988, and was promoted to an Associate Professor in

1994 and to a Professor in 2005. He has been engaged in the research on physical properties and applications of organic functional materials, particularly liquid crystals and conjugated polymers. He stayed in Physics Department at University of Utah from 1994 to 1995 as a visiting scientist and studied spectroscopy of conjugated polymers. He obtained Best Paper Award of Japan Liquid Crystal Society. His current research interests are nano-structured organic materials and their application to electronic and photonic devices.



Akihiko Fujii was born in Osaka, Japan in 1969. He received his B.E., M.E., and D.E. degrees from Osaka University in 1993, 1995, and 1997, respectively. After one-year JSPS fellowship, he joined Department of Electronic Engineering in Osaka University as a research associ-

ate in 1998, and was promoted to an Associate Professor in Division of Electrical, Electronic and Information Engineering, Graduate School of Engineering, Osaka University in 2006.

He has been engaged in research on optical and electrical devices utilizing organic materials including dye molecules and conducting polymers.

He is a member of the Japan Society of Applied Physics, the institute of Electrical Engineers of Japan, the Institute of Electronics, Information and Communication Engineers, and the Society of Polymer Science, Japan.